ISTANBUL TECHNICAL UNIVERSITY ★ GRADUATE SCHOOL

ANALYTICAL STUDIES ON THE HAND SPECIMENS FROM THE BLAGOJEV KAMEN W-AU ORE FIELD: AN APPROACH TO ITS ORE GENESIS

M.Sc. THESIS

Berk BAŞER

Department of Geological Engineering

Geological Engineering Programme

MAY 2022

ISTANBUL TECHNICAL UNIVERSITY ★ GRADUATE SCHOOL

ANALYTICAL STUDIES ON THE HAND SPECIMENS FROM THE BLAGOJEV KAMEN W-AU ORE FIELD: AN APPROACH TO ITS ORE GENESIS

M.Sc. THESIS

Berk BAŞER
(505181329)

Department of Geological Engineering

Geological Engineering Programme

Thesis Advisor: Prof. Dr. Emin ÇİFTÇİ

MAY 2022

ISTANBUL TEKNİK ÜNİVERSİTESİ ★ LİSANSÜSTÜ EĞİTİM ENSTİTÜSÜ

BLAGOJEV KAMEN W-AU CEVHER SAHASINA AİT EL ÖRNEKLERİNDE YAPILAN ANALİTİK ÇALIŞMALAR: CEVHER JENEZİNE BİR YAKLAŞIM

YÜKSEK LİSANS TEZİ

Berk BAŞER
(505181329)

Jeoloji Mühendisliği Anabilim Dalı

Jeoloji Mühendisliği Programı

Tez Danışmanı: Prof. Dr. Emin ÇİFTÇİ

MAYIS 2022

Berk BAŞER, a M.Sc. student of İTU Graduate School student ID 505181329, successfully defended the thesis entitled "ANALYTICAL STUDIES ON THE HAND SPECIMENS FROM THE BLAGOJEV KAMEN W-AU ORE FIELD: AN APPROACH TO ITS ORE GENESIS", which he prepared after fulfilling the requirements specified in the associated legislations, before the jury whose signatures are below.

Thesis Advisor : **Prof. Dr. Emin ÇİFTÇİ** ....
Istanbul Technical University

Jury Members : **Prof. Dr. Mustafa KUMRAL** ....
Istanbul Technical University

Prof. Dr. Nurullah HANİLÇİ ....
Istanbul University-Cerrahpaşa

Date of Submission : 27 April 2022
Date of Defense : 13 May 2022

To my beloved mother,

FOREWORD

I would first like to give my sincere thanks to my supervisor Prof. Dr.Emin Çiftçi for making me feel privileged to be his student and for letting me expand my knowledge of Geology in the Ore Deposits and Geochemistry area.

Prof. Dr. Sibila Borojević Šoštarić from the Department of Geological Engineering of the Univerity of Zagreb, to whom I feel indebted for accepting me as a contributor to one of her EIT projects, which I had the chance to write my thesis about. And also, a very special thanks to her Ph.D. student Tomislav Brenko and Master student Ana Anzulović for sharing their help and knowledge for my thesis.

I would also like to express my very gratitude to Prof. Dr. Nurullah Hanilçi and his Ph.D. student Fatih Özbaş from the Department of Geological Engineering of Istanbul University, who provided me with significant informations on the fluid inclusion studies.

Last but not least, my dear colleague Arzuman Rızvanoğlu has been very helpful as to giving his remarkable assistance for some of the aspects of my thesis work.

May 2022

Berk BAŞER
Geologist

TABLE OF CONTENTS

Page

ABBREVIATIONS

CBMP : Carpatho-Balkanian Metallogenic Province
DcMP : Dacian Metallogenic Province
DMP : Dinaric Metallogenic Province
EIT : European Institute of Technology
ICP-MS : Inductively Coupled Plasma–Mass Spectrometry
ICP-AES : Inductively Coupled Plasma–Atomic Emission Spectrometry
iTARG3T : Innovative Targeting & Processing of Tin, Tungsten, Tantalum Ores
ppl : Plane polarized light
ppm : Parts per million
REE : Rare Earth Element
SMM : Serbo-Macedonian Massif
SMMP : Serbo-Macedonian Metallogenic Province
TEMB : Tethyan - Euroasian Metallogenic Belt
TMC : Timok Magmatic Complex
wt. : Weight
xpl : Cross polarized light/Crossed polars
XRD : X-ray Diffraction

SYMBOLS

α	: Alpha sign
Δ	: Delta sign
§	: Top half section sign
T_e	: Eutectic temperature
T_h	: Homogenization temperature
T_m	: Last melting temperature

LIST OF TABLES

Page

LIST OF FIGURES

Page

ANALYTICAL STUDIES ON THE HAND SPECIMENS FROM THE BLAGOJEV KAMEN W-AU ORE FIELD: AN APPROACH TO ITS ORE GENESIS

SUMMARY

The Blagojev Kamen, a.k.a. Grabova Reka, deposit located in Eastern Serbia played a key role in the underground exploitation of the significant metals like W-Au and occasionally Sn and Ag in the 1950-1960s of Yugoslavia, which was later to be ceased. The mine is currently flooded.

So as to rekindle the expectancy for revealing the potential W-Au in the area, a comprehensive study has been conducted in the scope of iTARG3T (Innovative Targeting & Processing of W–Sn–Ta–Li Ores) project supported by EIT (European Institute of Technology).

The study area belongs in the orogenic belt of East Serbian Carpatho-Balkanides that spans through Romania, Serbia and Bulgaria, and is affiliated with the Neresnica-Beljanica metallogenic zone of Eastern Serbia. The metamorphic facies of green schist and amphibolite of Precambrian period and of Phanerozoic eon and mafic volcano-sedimentary sequence are intruded by Variscan granitoids that ultimately introduced a variety of metallic minerals into the system. These metamorphic facies mark a progressive increase in pressure and temperature southwards along the sampling locations. The host rock assemblages consist principally of chlorite schist, chloritic schist of an igneous origin and some meta-volcanoclastics. The prominent hydrothermal activities led to wolfram and gold mineralizations within quartz veins and stockworks along the fractures of green schist. The placer gold obtained that were obtained along the River Pek values up to 30g/ton (10g/ton on average), and WO_3 content varies between 0.2 and 2.0 wt. %. In the vicinity of the study area are also Pb-Zn ore bodies which are believed to have contaminated the W-Au bearing quartz veins judging by the peak anomalies observed in the geochemical analyses.

A total of twenty hand specimens have been procured from the outcrops that are situated in the vicinity of Blagojev Kamen in order that their mineralogical, petrographical and geochemical characteristics could be revealed via analyses.

To start off, rock samples that might have had the possibility of bearing important metallic minerals have been determined and analyzed. The sample T10-D has showed a notable concentration for the manganese dioxide mineral termed pyrolusite in the XRD profile. According to the XRD analyses, four major alteration types have been characterized: (1) Propylitic (quartz, Ca-rich albite, Ca-rich anorthite, pargasite, ferropargasite, dravite (Mg-rich tourmaline), tremolite (amphibole group), phlogopite (end-member of biotite), clinochlore (chlorite), montmorillonite and epidote; (2) argillic (quartz, muscovite mica and clay minerals); (3) sericitic (phyllic) (quartz and muscovite mica); (4) potassic (quartz, K-feldspar, biotite and anorthite). In addition, pyritization and sericitization have been distinguished in the select samples.

Pyrite, chalcopyrite, goethite, sphalerite, ilmenite (?) and pyrolusite minerals have been encountered in the polished sections of the green schist and amphibolite under the ore microscopy. Pyrite, being the most abundant, usually has euhedral to subhedral cubic crystal structures, while showing off a epigenetic cataclastic texture in one of the sections. The pyrolusite anomaly seen in the XRD diffractogram has been verified by microscopic observations, as well. Sphalerite shows as a replacement product of pyrite and on occassion, of chalcopyrite.

The chemical compositions of the metamorphic rock samples have been found out. The results yielded very low concentrations of W (9.28 ppm on average) and Mn (1052 ppm on average) meanwhile Au has been detected in none of the samples. A small amount of Pb concentration could be attributed to the contamination from the neighbouring Pb-Zn ore bodies.

Stable isotope analyses for S and O isotope ratios have been carried out. $^{34}S/^{32}S$ (pyrite) and $^{18}O/^{16}O$ (quartz) values for the Blagojev Kamen deposit correspond to an average of 2.15‰ and 11.60‰, respectively. $\delta^{18}O_{water}$ has been calculated to be 3.24‰ and δD_{water} to be 35.92‰. Based on these values and assumptions, the sulfur-rich fluids have an igneous origin while the water that contributed to the precipitation of the metallic ore minerals originated from a metamorphic genesis.

For the purpose that the salinity and temperature conditions of the ore-bearing fluids could be presented, fluid inclusion studies have been conducted on the quartz minerals of the hand specimens. The measurement results indicated a low to intermediate salinity window (2.57 – 13.29 equiv. wt.% NaCl) and an intermediate homogenization temperature range (186.1 ºC – 390.3 ºC) for primary inclusions. The T_h-Salinty plot of both primary and secondary inclusions illustrated that a likely retrograde boiling event might have occurred during the mineralization stage of the metallic ore minerals. However, some inclusions have been interpreted to contain a noticeable CO_2-Clathrate gas combination as the T_m values for these inclusions fall in the +0 ºC - +10 ºC array. Utilizing the thermal profiles correlated with vapor pressures and densities, the following factors for the Blagojev Kamen W-Au deposit have been deduced: (1) Fluid pressure≈ 61 bar (6.1 MPa); (2) Fluid depth≈ 695m; and (3) Fluid density≈ 0.82 g/cm^3.

The crucial mechanism behind the W-Au mineralization for the Blagojev Kamen deposit is believed to be interconnected with regional metamorphism that caused the ore-forming solutions to be transported through fractures and micro-cracks in the host rock.

BLAGOJEV KAMEN W-AU CEVHER SAHASINA AİT EL ÖRNEKLERİNDE YAPILAN ANALİTİL ÇALIŞMALAR: CEVHER JENEZİNE BİR YAKLAŞIM

ÖZET

Doğu Sırbistan'da bulunan Blagojev Kamen, diğer adıyla Grabova Reka, 1950-1960'larda Yugoslavya'nın W-Au ve yer yer Sn ve Ag gibi önemli metallerin yeraltında işletilmesinde önemli bir rol oynadı ve bu maden daha sonra durduruldu. Şu anda maden su basmış bir halde bulunmaktadır.

EIT (Avrupa Teknoloji Enstitüsü) tarafından desteklenen iTARG3T (İnovatif Hedefleme ve W–Sn–Ta–Li Cevherlerinin İşlenmesi) projesi kapsamında, bölgedeki potansiyel tungsten ve altın birlikteliklerinin ortaya çıkarılmasına yönelik beklentiyi yeniden canlandırmak amacıyla kapsamlı bir çalışma yürütülmüştür.

Çalışma alanı, Romanya, Sırbistan ve Bulgaristan'ı kapsayan Doğu Sırp Karpato-Balkanitlerinin orojenik kuşağına aittir ve Doğu Sırbistan'ın Neresnica-Beljanica metalojenik bölgesine bağlıdır.

Geçmişte, Blagojev Kamen ve yakın lokalitelerinde altın ± şeelit yataklarının ekonomik değere sahip olduğu kaydedilmiştir. Erken Paleozoik mafik volkano-tortul kompleksinde ve yeşil şistte çok sayıda şeelit içerikli kuvars-altın damarları bulunmaktadır. Cevher damarları yeşil şist foliyasyonları boyunca oluşmuştur. Nabit altın ve şeelit, ana cevher mineralleri olarak gözlemlenirken, minör pirit (bazen yeşil şistte bulunur) ve bunlara eşlik eden tali sfalerit, galen ve nadiren de pirarjirit bulunmaktadır. Tartışmalı olarak, birincil safhada oluşmuş olan altının volkano-sedimanter kökenli olduğu düşünülmektedir.

Pek deresindeki Kuvaterner çökelleri, nihayetinde plaser altın çökelimini ve Neresnica granitoidi üzerinde oluşan plaserde monazitin varlığını ortaya koymaktadır. Literatürde, bu altın alüvyon plaserlerinin Blagojev Kamen cevher sahasına ait kuvars damarlarından dere suyu tarafından taşındığı ve çökeldiği belirtilmektedir.

Prekambriyen dönemine ve Fanerozik çağa ait yeşil şist ve amfibolit metamorfik fasiyesleri ve mafik volkano-tortul sekansı, nihayetinde sisteme çeşitli metalik mineraller katan Variskan granitoyidleri tarafından kesilmiştir. Bu metamorfik fasiyesler, alınan numunelerin lokasyonları boyunca güneye doğru basınç ve sıcaklıkta kademeli bir artışa işaret etmektedir. Ana kayaç toplulukları esas olarak klorit şist, magmatik kökenli kloritik şist ve bazı meta-volkanoklastiklerden oluşmaktadır. Öne çıkan hidrotermal faaliyetler, yeşil şistteki kırık ve çatlaklar boyunca kuvars damarlarında ve ağsı yapılarda tungsten ve altın cevherleşmelerine yol açmıştır. Bu damarlar 0,2 m ila 1.1 m kalınlıkta ve 100 m ila 200 m arasında uzukluklara sahiptirler. Tüm damar mineralizasyonlarında piritleşmeye rastlanılmaktadır. Çoğu kez ana kaya litolojisi, magmatik kökenli klorit şist ve kloritik şist ve meta-volkanoklastikler (meta-volkan-tortul) olarak gözlenmektedir.

Pek deresi boyunca alınan el örneklerinde plaser altın değerleri 30 g/ton'a kadar (ortalama 10 g/ton) ve WO_3 içeriği ise ağırlıkça 0,2 ile 2,0 % arasında değişmektedir.

Jeokimyasal analizlerde gözlemlenen konsantrasyonuna bakılınca, inceleme alanının yakınlarında bulunan Pb-Zn cevher kütlelerinin W-Au içeren kuvars damarlarını kontamine ettiği düşünülmektedir.

Blagojev Kamen civarında yer alan mostralardan toplam yirmi adet el numunesi mineralojik, petrografik ve jeokimyasal özelliklerinin analizlerle ortaya konabilmesi için temin edilmiştir.

İlk olarak, önemli metalik mineralleri barındırma olasılığına sahip olabilecek kayaç örnekleri tespit edilmiş ve X-ışını difraktometresi ile analiz edilmiştir. T10-D numunesi, XRD çözümlemesinde pirolüzit olarak adlandırılan manganez diyoksit minerali için dikkate değer bir konsantrasyon göstermiştir. XRD analizlerine göre, dört ana alterasyon tipi karakterize edilmiştir: (1) Propilitik (kuvars, Ca bakımından zengin albit, Ca bakımından zengin anortit, pargazit, ferropargazit, dravit (Mg bakımından zengin turmalin), tremolit (amfibol grubu), flogopit (biyotitin son üye minerali), klinoklor (klorit), montmorillonit ve epidot; (2) arjilik (kuvars, muskovit mika ve kil mineralleri); (3) serisitik (fillik) (kuvars ve muskovit mika); (4) potassik (kuvars, K-feldispat, biyotit ve anortit). Ayrıca, seçilmiş örneklerde piritleşme ve serisitleşme gözlemlenmiştir.

Cevher mikroskobunda yeşil şist ve amfibolitin parlak kesitlerinde pirit, kalkopirit, götit, sfalerit, ilmenit (?) ve pirolüzit minerallerine rastlanmıştır. En bol bulunan pirit, genellikle özşekilli ile yarı özşekilli kübik kristal yapılara sahiptir ve parlak kesitlerin birinde epijenetik kataklastik bir doku sergilemektedir. XRD difraktogramında gözlemlenen pirolüzit anomalisi, mikroskobik incelemeler ile de doğrulanmıştır. Sfalerit, piritin ve bazen de kalkopiritin ornatım ürünü olarak görülmektedir.

Metamorfik kayaç örneklerinin jeokimyasal bileşimleri tespit edilmiştir. Sonuçlar çok düşük konsantrasyonlarda W (ortalama 9.28 ppm) ve Mn (ortalama 1052 ppm) göstermiştir ve ayrıca örneklerin hiçbirinde Au değerine rastlanılmamıştır. Az miktarda bulunan Pb konsantrasyonu, komşu Pb-Zn cevher kütlelerinden kaynaklanan kontaminasyona atfedilebilir.

S ve O izotop oranlarının tespiti için kararlı izotop analizleri yapılmıştır. Blagojev Kamen cevher yatağı için $^{34}S/^{32}S$ (pirit) ve $^{18}O/^{16}O$ (kuvars) değerleri ortalama 2,15‰ ve 11,60‰'a karşılık gelmektedir. Sırasıyla, $\delta^{18}O_{su}$ 3,24‰ ve δD_{su} 35,92‰ olarak hesaplanmıştır. Bu değerlere ve varsayımlara dayanarak, kükürt bakımından zengin akışkanlar magmatik bir kökene sahipken, metalik cevher minerallerinin çökelmesine katkıda bulunan su, metamorfik bir oluşumdan gelmektedir.

Cevherli akışkanların tuzluluk ve sıcaklık koşullarının ortaya konulması amacıyla, çalışma alanından alınan metamorfik kayaların kuvars mineralleri üzerine sıvı kapanım çalışmaları yapılmıştır. Ölçüm sonuçları, birincil kapanımlar için düşük ila orta tuzluluk değerlerine (2.57 – 13.29 eşdeğer ağırlıkça NaCl) ve orta derece homojenizasyon sıcaklık aralığına (186.1 ºC – 390.3 ºC) işaret etmiştir. Hem birincil hem de ikincil kapanımların T_h-Tuzluluk grafiği, metalik cevher minerallerinin mineralizasyon aşaması sırasında olası bir geriye dönük kaynama olayının meydana gelmiş olabileceğini göstermiştir. Bununla birlikte, bazı kapanımların T_m değerleri +0 ºC – ila +10 ºC aralığında yer aldığından dolayı bu kapanımlarda mevcut bir CO_2-Klatrat gaz karışımının varlığına yorumlanmıştır. Buhar basınçları ve yoğunlukları ile ilişkili termal profiller kullanılarak, Blagojev Kamen W-Au cevher yatağı için şu faktörler ortaya konmuştur: (1) Akışkan basıncı≈ 61 bar (6,1 MPa); (2) Akışkan derinliği≈ 695m; ve (3) Akışkan yoğunluğu≈ 0,82 g/cm3.

Blagojev Kamen yatağınındaki W-Au cevherleşmesinin arkasındaki önemli mekanizmanın, cevher oluşturan çözeltilerin ana kayadaki kırıklar ve mikro çatlaklar yoluyla taşınmasına sebebiyet veren bölgesel metamorfizm ile ilişkili olduğuna inanılmaktadır.

1. INTRODUCTION

1.1 General Information

The geological environment of Serbia is quite complicated. Its characteristics show a large quantity of rock formations of different lithological composition, petrochemical features, age and metallogenic specialization.

The mineral resources of Serbia and the metollogenic or tectonic units where they are situated are constituent parts of regional metallogenic and geotectonics units greater than its territory. Correspondingly, the position, time and condition of the formation of the mineral resources of Serbia are strictly dependent on a huge extent on the geotectonic evolution of that vast territory and the contributive volcanic, sedimentary and metamorphic processes. The significance of the mineral deposits in the aforementioned metallogenic and geotectonic units vary depending on their territorial distribution, their type and environment, the range of their formations, the association of the ore and accompanying elements, and the chronological history of their formation.

The metallogenic zones of Serbia encompass important metallic and non-metallic mineral deposits depending on their tectonic settings and fluid compositions, many of which are copper, gold, iron, lead-zinc, manganese, wolfram, molybdenum, nickel, tin, antimony, bismuth, chromium, bauxite, uranium, titanium, etc.

The study area of the thesis is in the Blagojev Kamen wolfram-gold ore field located in the eastern part of Serbia. Blagojev Kamen ore field has been documented to be under mining operations up until the year 1963, producing gold and wolfram and is currently flooded.

The village of Blagojev Kamen is located in the municipality of Kučevo in the Braničevo District of eastern Serbia and its geographical coordinates are 44^{o} 26' 15" in latitude and 21^{o} 51' 23" in longitude. Braničevo District is surrounded by the rivers Danube and Great Morava and the mountain range of Homolje mountains, Beljanica and Kučevo mountains to the south. Municipality of Kučevo is at an altitude of 120 to

920 meters above sea level. It has, in most cases, a hilly to mountainous area. The municipality has 56,734 residents. Blagojev Kamen village is inhabited by so low as 38 people, where is also located by the river Pek, a 129 km long tributary of Danube. It was named after the former gold mine that had been operated between the years 1902 and 1963.

The village lies about 12-15 km northwest from the Majdanpek copper-gold-silver open pit mine and approximately 5-8 km southeast from the Markova Krčma mountain (Figure 1.1).

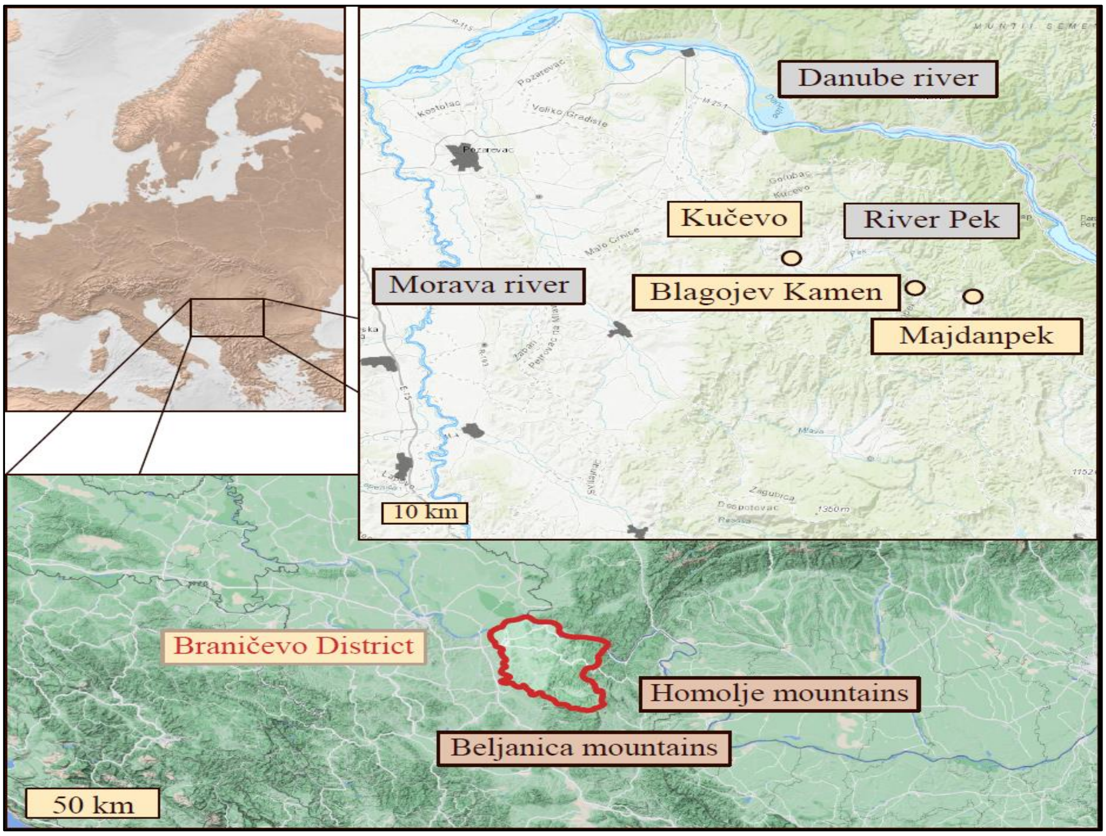

Figure 1.1 : Google Maps footage of the geographical location of the study area (Anzulović, 2022).

1.2 Aim of the Study

This thesis is affiliated with an ongoing EIT (European Institute of Technology) project that is named iTarg3t which focuses its prospection on the tin-wolfram-lithium-tantalum deposits of Europe. Accordingly, this thesis work aims to shed light on the current possibility of further profiting from the Blagojev Kamen gold-wolfram ore field, where the underground mining operations had been ceased following the year 1963.

2. MATERIALS AND METHODS

2.1 Field Work

First off, a comprehensive in-situ field work could not be realized due to the current Covid-19 pandemic restrictions and the close-off of the borders of Serbia that is still in effect. For this reason, only the hand specimens garnered prior to the Covid-19 situation were considered to be relevant materials for evaluation.

Blagojev Kamen gold-wolfram ore field belongs in the north of the Neresnica-Beljanica metallogenic zone, where is due northwest of the Carpatho-Balkanian metallogenic province. The aimed W, Au–W and Au–Ag–W mineralizations in the Proterozoic metamorphic units in locality of Blagojev Kamen have been inspected in the Pek riverbed, in the vicinities of the adit and waste rock dumps of the old underground mines.

In total, twenty hand specimens were procured from the outcrops of the ore field, covering approximately 4,5 km south of Blagojev Kamen village, following up circa 8,5 km north, sixteen of which were sent to Istanbul Technical University for petrographic, XRD, fluid inclusion, stable oxygen and sulfur isotope analyses. The samples were labeled with ES-T and numbered beginning from 1 to 20. The locations of the previous mining activities have been taken as a reference while sampling in order to pinpoint the ore anomalies.

A detailed geological map of the area is shown in Figure 2.1.b. The selected sixteen samples have been divided respectively into three different categories according to their petrographic characteristics and the metamorphic units they belong to, and are specified on the geological map of the area (Figure 2.1.b):

1) ES-T3, T4, T5, T9, T10-A2, T10-A3, T10-B, T10-D, T10-F2, T10-E2, T11, T12-1 – Quartz vein, muscovite-garnet-quartz schist, quartz-muscovite schist, muscovite schist, schist, altered quartz vein, pyrite-rich quartz vein, gneiss, amphibolite, quartz vein, sericite schist, pegmatitic garnet-quartz-feldspar-muscovite schist

2) ES-T15-B2, T15-B5 – Quartz vein, quartz-muscovite schist

3) ES-T20-1, T20-3 – Quartz vein, muscovite schist

The macrophotographs of the hand specimens are showcased in Figure 2.2; 2.3; 2.4; 2.5; 2.6; 2.7.

The geological cross-section of the study area is presented in Figure 2.8. Locations of the ore vein mineralizations were taken as reference points for charting the cross-section.

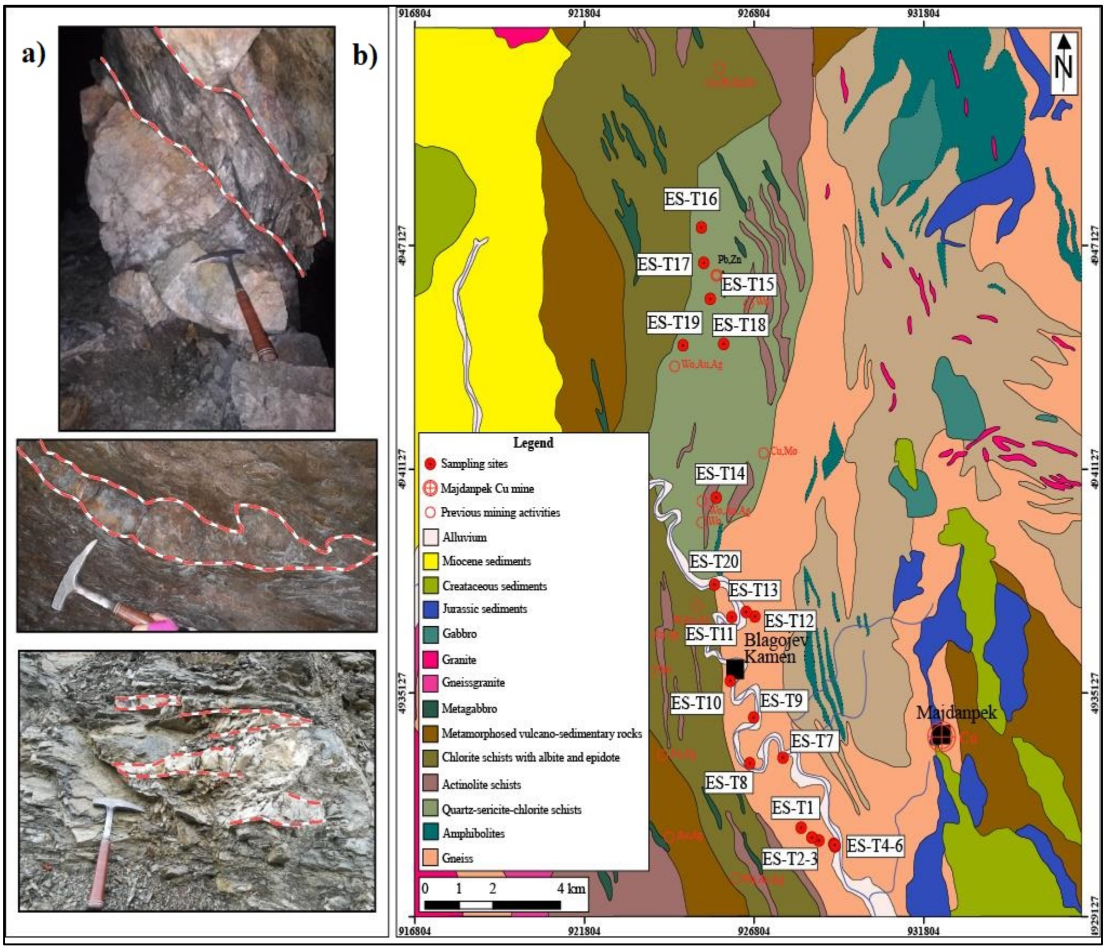

Figure 2.1 : a) Macrophotographs of the quartz veins containing metallic sulfide minerals; b) geological map of the study area. Dotted red circles illustrate the sampling locations. Previous mining activities are shown in red circles (modified after Kalenić and Hadži–Vuković, 1978).

Sample Macrophotograph | **Description**

Sample ES-T3
Quartz vein
-~4cm in length
-Reddish pink colored
-Hard

Sample ES-T4
Muscovite-garnet-quartz schist
-~4cm in length
-Olive green colored
-Very hard

Figure 2.2 : Macrophotographs of the hand specimens ES-T3 and ES-T4.

Sample Macrophotograph | **Description**

Sample ES-T9
Muscovite schist
-~6cm in length
-Brown colored
-Very hard

Sample ES-T10A-2
Schist
-~5cm in length
-Creamy green colored
-Brittle

Sample ES-T10A-3
Altered quartz vein
-~2.5cm in length
-Dark brown colored with reddish tint
-Very hard to brittle

Figure 2.3 : Macrophotographs of the hand specimens ES-T9, ES-T10A-2 and ES-T10A-3.

Sample Macrophotograph	**Description**
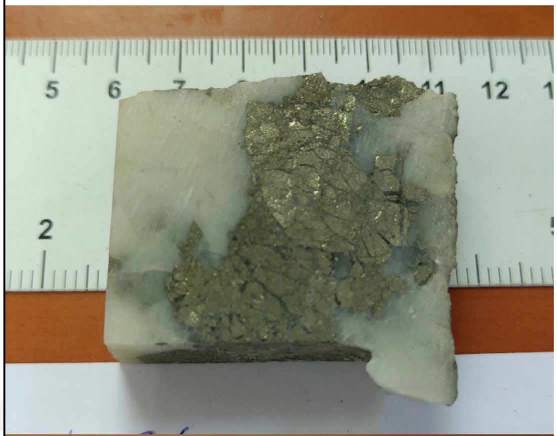	**Sample ES-T10-B** **Quartz vein** **-~5cm in length** **-Creamy white colored** **-Hard** **-Visible pyrite occurences**
	**Sample ES-T10-D** **Gneiss** **-~7cm in length** **-Brown colored with reddish tint** **-Very hard**
	**Sample ES-T10E-2** **Amphibolite** **-~6cm in length** **-Dark green colored** **-Hard** **-Visible pyrite occurrences**

Figure 2.4 : Macrophotographs of the hand specimens ES-T10-B, ES-T10-D and ES-T10E-2.

Sample Macrophotograph | **Description**

Sample ES-T10F-2
Quartz vein
-~3.5cm in length
-Creamy white colored with brownish tint
-Hard

Sample ES-T11
Sericite schist
-~6.5cm in length
-Light green with yellowish tint
-Very hard

Sample ES-T12-1
Pegmatitic garnet-quartz-feldspar-muscovite schist
-~5cm in length
-Light to dark green colored
-Moderately hard to brittle

Figure 2.5 : Macrophotographs of the hand specimens ES-T10F-2, ES-T11 and ES-T12-1.

Sample Macrophotograph	**Description**
	**Sample ES-T15B-2** **Quartz vein** **-~4cm in length** **-White to green colored with brownish tint** **-Hard**
	**Sample ES-T15B-5** **Quartz-muscovite schist** **-~4 and 3cm in length** **-Dark green with brownish tint** **-Brittle**
	**Sample ES-T20-1** **Quartz vein** **-~4cm in length** **-White to creamy white colored** **-Brittle**

Figure 2.6 : Macrophotographs of the hand specimens ES-T15B-2, ES-T15B-5 and ES-T20-1.

Sample Macrophotograph	**Description**
	**Sample ES-T5** **Quartz-muscovite schist** **-~4.5cm in length** **-Light green colored with brownish tint** **-Brittle**
	**Sample ES-T20-1** **Muscovite schist** **-~5cm in length** **-Light green colored** **-Hard**

Figure 2.7 : Macrophotographs of the hand specimens ES-T5 and ES-T20-1.

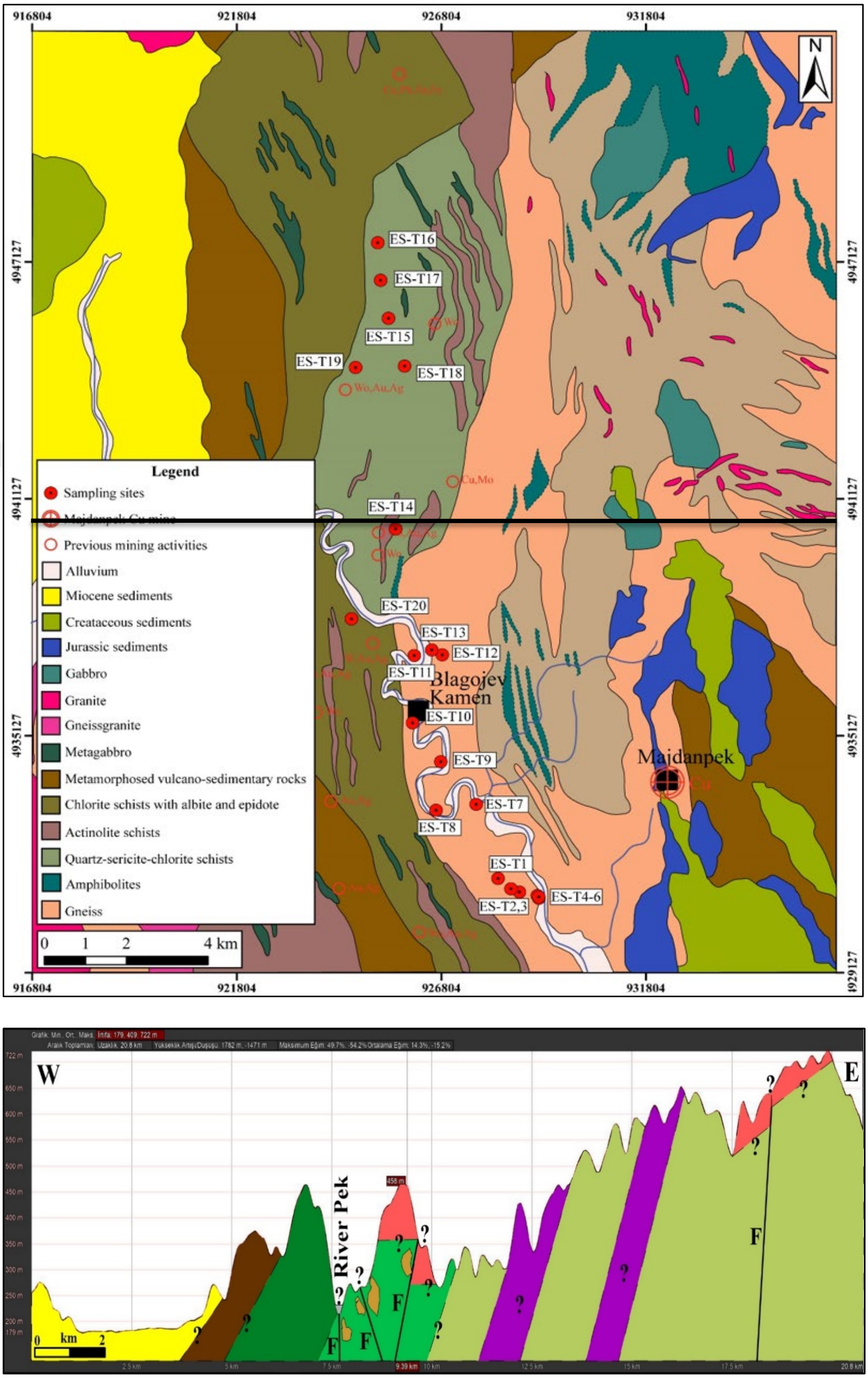

Figure 2.8 : Geological cross-section of the study area (from west towards east).

2.2 Laboratory Studies

Besides the petrographic assessments, XRD, ICP-MS, ICP-AES, fluid inclusion and stable oxygen and sulfur isotope analyses were also conducted on the samples collected from the Blagojev Kamen ore field and its outskirts.

2.2.1 Petrographic assessments

Petrographic studies have been carried out at Zagreb University and Istanbul Techincal University. The polished thin sections were prepared in the thin section and polishing laboratories of both universities. The hand specimens were inspected by naked eye and marked in part in order to determine the possible ore enrichments. Following this process, the determined parts were cut with the help of diamond cutters. The cut pieces were chipped with a surface area of 1.5 x 2 cm and a thickness of about 1-2 cm. Before the chips were placed in the polished section preparation mold, they had been coated with vaseline in order that the samples should come out easily after drying. The samples were frozen up in the mold with the material called epoxy. Sandpaper No. 180 was used for the first rough smoothing process, and then sandpapers No. 320, 600, 800 and 1000, respectively, were used in the automatic polishing device. Petrographic examination of the samples was carried out on microscope Leica Microsystem 020–522 101 DM/LSP at the Faculty of Mining, Geology and Petroleum Engineering of University of Zagreb. The brand and model of the camera is Canon CA–PS700. Ore mineralogy of the samples was inspected on Leica DM4500P polarization microscope over a Leica branded camera.

2.2.2 XRD analyses

X-ray diffraction analyses were conducted on the relevant rock samples in the XRD laboratories of the Geological Engineering Department at the University of Zagreb and Istanbul Technical University so as to determine their mineralogical compositions through X-ray diffractograms. Prior to realizing that, three different rock samples (quartz vein, chlorite schist and gneiss) mustered from the allocated locations were crushed with hammer and sieved to certain grain sizes, which are 2 mm-1 mm; 1mm-0.5 mm; 0.5 mm-0.25 mm; 0.25 mm – 0.125 mm; < 0.125 mm from the coarsest to the finest in order. The purpose was to neatly select and collect the purest samples as possible under stereo microscope (Figure 2.9).

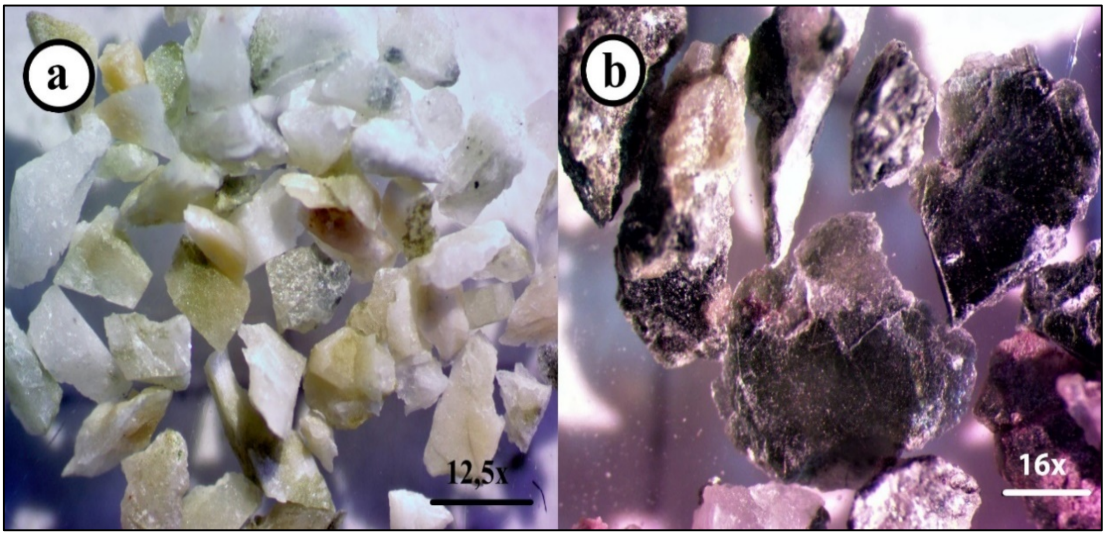

Figure 2.9 : Sample photographs taken under stereo microscope. a) Selection of pink and white colour fragments of sample 7575; b) tweezers-picked green colour fragments of sample 7558.

With sufficient amount of sample collections, mortar and pestle was used to grind them over to fine powder size and these collections were poured into small paper bags with different labeling for each one. XRD analyses then were run on D8 ADVANCE BRUKER-XRD with an XRD operating power of 3KeV-30KeV, outputting five distinctive diffractograms, three of which were previously subdivided according to their colors (white, green and pink).

2.2.3 ICP-MS and ICP-AES analyses

In this part of the study, ICP-MS (Inductively coupled plasma–mass spectrometry) and ICP-AES (Inductively coupled plasma–atomic emission spectrometry) instruments have been used at the recognized MS Analytical Laboratory in Langley, Canada, in order to determine the multi-elemental compositions and the oxide minerals of the targeted samples. REE values are also included in the analysis results.

Multielement contents have been analysed using inductively coupled plasma–mass spectrometry (ICP–MS) by applying a 4–acid digestion including hydrochloric, nitric, perchloric and hydrofluoric acids. These types of acids were used for achieving near total digestion.

Analysis for major oxides have been performed using powdered samples which were analysed with inductively coupled plasma–atomic emission spectrometry (ICP–AES) plying lithium borate ($LiBO_2$) fusion. Loss on ignition (LOI) was regulated by weight difference after ignition at 1000 °C.

2.2.4 Fluid inclusion studies

It is widely known that the fluid inclusion subject holds import as to helping define the origin of rock fluid. Hence, this study has been thoroughly conducted on Linkam THMSG-600 Geology Stage with a built-in Leica 2500DM polarization microscope in the Advanced Microscopy Laboratory of the Mining Faculty of Istanbul Technical University. Five particular double-polished wafers were prepared out of quartz-bearing hand specimens in thin the section and polishing laboratory of the university. As in the polished thin sections, the same marking procedure was applied on the quartz minerals. These markings were cut with the help of a diamond cutter. Each cut sample was first etched in 220 grit, then 600 grit and finally 1000 grit. All abraded specimens were polished for at least 5 minutes with the help of Al_2O_3 powder. Then, all the polished sections were left to dry in room temperature for one daytime. After the drying process was completed, each sample was cut to a height of 1 mm in a diamond cutter to polish the other surfaces of the samples in the same way. After the cutting processes, the other surfaces of the samples were also polished likewise.

2.2.5 S and O isotope analyses

This study includes two different genres of stable isotope analyses, namely the $\delta^{34}S$ and $\delta^{18}O$, that were conducted on the select samples of the Blagojev Kamen deposit at the Department of Geology of the University of Georgia, U.S.A.. Necessary samples have been determined and collected under the stereo microscope for interpretation and analysis (Figure 2.10).

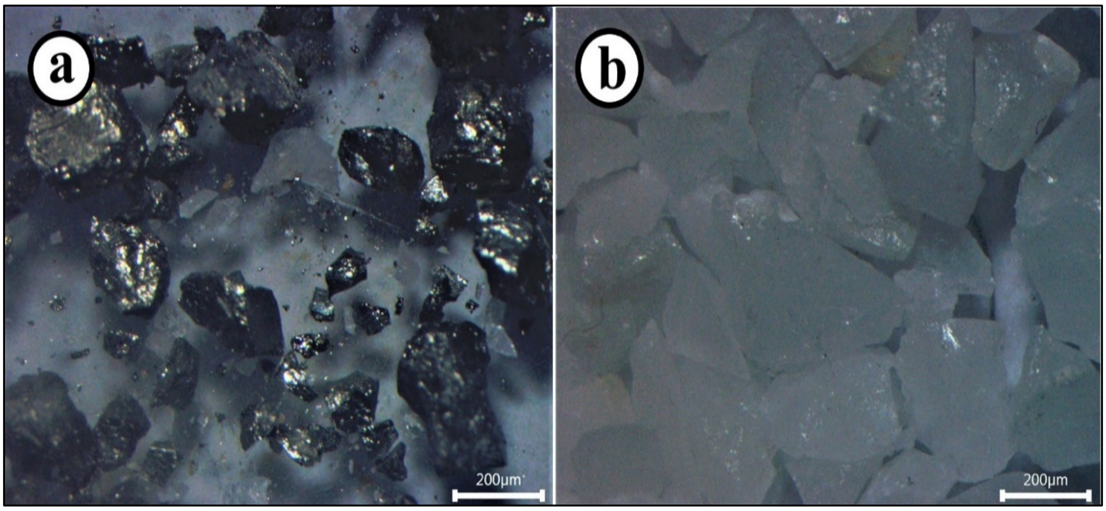

Figure 2.10 : Sample images for isotope analysis. a) T10-E2 - pyrite; b) T15-B2 – quartz.

For the sulfur isotope analysis, prepared ore samples were analyzed by EA-IRMS method. In this method, the samples interact with vanadium pentoxide and oxygen vapor, and the quartz tube is rapidly cooled to room temperature to prevent the formation of sulfur trioxide. This analysis can be done by producing 0.2 mg of sulfur dioxide from approximately 25 mg of sulfates and 5-12 mg of sulfides.

For the oxygen isotope analysis, SiO_2 was transformed into CO_2 at varying powers (Synard, 10510-10650nm wavelength, 75W max power) with BrF_5 under vacuum and analyzed in Finnigan MAT 252 mass spectrometer.

3. GEOLOGICAL SETTING

3.1 Tectonism

Serbia has a quite complex geological setting that encapsulates a huge number of rock formations of different lithological composition, petrochemical characteristics, age and metallogenic occurences.

The mineral resources of Serbia cover a vast territory where their formations are inter-related with the very metallogenic and tectonic units. Correspondingly, the geotectonic evolution of this territory guided the position, time and conditions of the formation of the mineral resources of Serbia, following the volcanic, sedimantary and metamorphic processes. The significance of the mineral deposits in the aforementioned metallogenic and geotectonic units differs in relation with their territorial placement, their type and circumference, the coverage of their occurences, the relationship with the ore and backing elements, and the chronological range of their formation (Jelenković et al, 2008).

Geological history of the South–Eastern Europe is dominated by the single Tethys ocean (Schmid et al., 2008; Borojević Šoštarić et al., 2014) or multiple oceans (Pamić et al., 2002; Karamata, 2006) in–between the Eurasia and Gondwana.

Pre–Tethyan geological evolution corresponds to a period from Precambrian to Mesozoic times. On the European side it is introduced by three tectonic continental blocks: the Moesian Platform, the Tisza–Dacia Mega–Unit and the Rhodopes. On the Gondwanan part is the Adriatic microplate that was later included to External Dinarides, the Dalmatian–Ionian Zone and Stable Adria. The Moesian Platform is the stable margin of Europe since the Jurassic Cimmerian orogeny and can be regarded as “undeformed European foreland” (Schmid et al., 2008). The Moesian Platform includes Neoproterozoic metamorphic rocks that locally show a Variscan overprint (Seghedi et al., 2005; Oczlon et al., 2007) and it is usually covered by younger sediments. The Tisza–Dacia Mega–Unit is the area between the eastern border of the mega–suture or the Eastern Vardar and the Moesian Platform. It consists of two nappe systems, the Serbo–Macedonian Massif and the Carpatho–Balkanides.

The Tisza Unit (Prinz, 1926) is a lithospheric fragment bound by the Mid–Hungarian Lineament (Fülöp, 1989) to the north–west, the Sava, Sombor–Bečej and Mureş Lineament (i.e. the north–western border of the Srem–Mureş Ophiolite belt) to the south and the Someş Lineament to the north–east (Haas and Péró 2004). Owing to similarities in the crystalline basement, lithofacies and fossil assemblage between specific parts of the Tisza Unit and the Western Carpathian units it is presumed that Tisza Unit could be considered a continuation of the Inner Carpathian units (Kovács, 1984; Kovács et al., 1989; Haas et al., 1990). The basement outcrops of the Tisza Unit occur in the Slavonian Mountains–Moslavačka Gora, Papuk, Psunj, Krndija (Balen et al., 2006; Pamić et al., 2002), in the South Transdanubian ranges and in the Apuseni Mountains (Haas and Péró 2004).

The Tisza Unit broke off from the southern margin of the European plate during the Middle Jurassic (Channell and Horvath 1976; Balla and Bodrogi 1993; Kovács et al., 1989) and it has a rather sophisticated movement history and multiple translations and rotations during Mesozoic and Cenozoic times (Csontos, 1995). In the Variscan and early Alpine evolutionary stages the Variscan terrane accretion was accompanied by rigorous deformation and progressive regional metamorphism. This was followed by transpressional tectonics in the late and post–Variscan stages, leading to the development of molasse basins (Haas and Péró 2004). In the mid–Cretaceous, due to the northward motion of the Adria Block and related west to east closure of the westernmost Neotethys basin, and the eastward motion of Moesia, the extensional regime switched to compressional. This alternation led to the onset of nappe stacking and low–grade regional metamorphism within the Tisza Unit (Haas and Péró 2004). In the early Tertiary the north–eastward interactive motion of the Alcapa and Tisza Dacia Blocks led to the formation of the heterogeneous basement of the Pannonian Basin (Csontos et al., 1992).

The Rhodope massif is the internal Europe–derived geological unit that underwent high to ultra–high pressure metamorphism and was afterwards overprinted by granulite and amphibolite facies (Cvetković et al., 2016).

The Syn–Tethyan geology encapsulates geological units, which record the former existence of the Mesozoic oceanic lithosphere, generally being represented by ophiolites and trench/accretionary wedge assemblages to date, formed and reworked in the course of the Tethys Ocean lifespan. Ophiolitic belt is termed the Vardar–Tethyan mega suture (Cvetković et al., 2016). In the Vardar–Tethyan mega suture, three subparallel belts can be observed, commonly called Dinaric, Western Vardar and Eastern Vardar ophiolitic units (Borojević Šoštarić et al., 2014).

The Post–Tethyan geology includes rocks that are stratigraphically overlying the Vardar–Tethyan mega suture zone and identifies as rapid extension and exhumation, high heat flow, magmatism and lithosphere thinning (Cvetković et al., 2016).

Serbia is of five major geotectonic units within its territory: Dinarides, Vardar Zone, Serbo-Macedonian Massif (SMM), Carpatho-Balkanides and Pannonian Basin (Dimitrijević, 1982; 1997). These geotectonic units are all part of the Tethyan-Euroasian Metallogenic Belt (TEMB), or on a wider scale namely the North-Eastern Mediterranean Sector (Janković, 1967; 1974; 1990; 1997).

The Tethyan-Euroasian metallogenic belt, being the largest orogenic belt on Earth, extends from Europe throughout Anatolia to Pacific Ocean and possesses one of the most economic metallogenic zones due to its geodynamic mobility. A simplified tectonic map of the Tethyan orogenic belt illustrates that the Carpatho-Balkanian tectonic unit is subject to a subduction-related thrust faults along the territory (Figure 3.1). Blagojev Kamen ore district accordingly belongs to the Carpatho-Balkanian tectonic unit and is topografically adjacent to the Serbo-Macedonian Massif on geological scale.

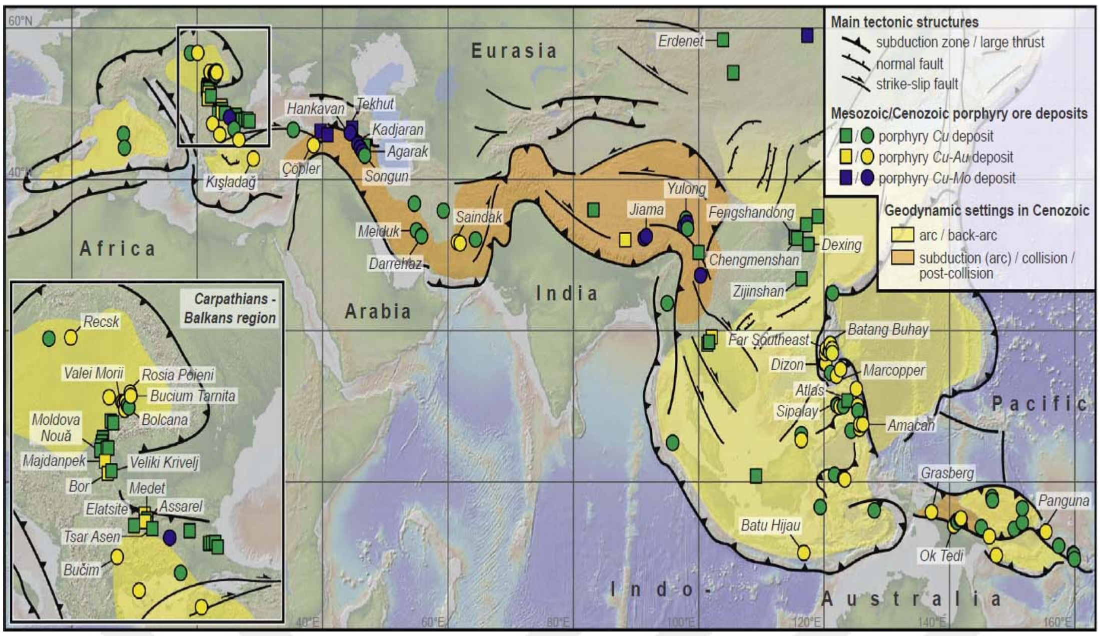

Figure 3.1 : Simplified tectonic map of the Tethyan orogenic belt showing the main tectonic structures and geodynamic settings in Cenozoic era. Arc/back-arc and arc/collision/post-collision settings occurring along this belt are as well witnessed. Detailed map of the Carpatho-Balkanide region is shown in lower-left corner. Locations and ages of ore deposit are obtained from Singer et al., (2008); Cassard et al., (2012); Richards (2014); Delibaş et al., (2016a); Moritz et al., (2016).

3.2 Origin and Evolution of Mineralization

Based upon the statements of Jelenković et al. (2008), all mineral deposits and occurrences in Serbia gather under four regional metallogenic provinces spanning beyond the territorial boundaries of the country: (1) The Dinaric metallogenic province (DMP) encapsulating the western part of Serbia; (2) The Carpatho-Balkanian metallogenic province (CBMP) in the north-eastern part of Serbia; (3) The Serbo-Macedonian metallogenic province (SMMP) in the central part of Serbia, representing the terrains of the Vardar Zone, the Serbo-Macedonian Massif and the eastern part of Dinarides; (4) The Dacian metallogenic province (DcMP) that encompasses a rather small area in the far north-eastern part of Serbia. The Dinaric, Serbo-Macedonian and Carpatho-Balkanian metallogenic provinces can be subdivided into sundry metallogenic zones, ore districts and ore fields, some of which are of certain characteristics related with the origin of the deposits.

In order to depict the metallogenic provinces and zones mentioned above, a simplified metallogenic map of Serbia with its mineral deposits and many other metallic and industrial mineral occurrences of importance is presented in Figure 3.2.

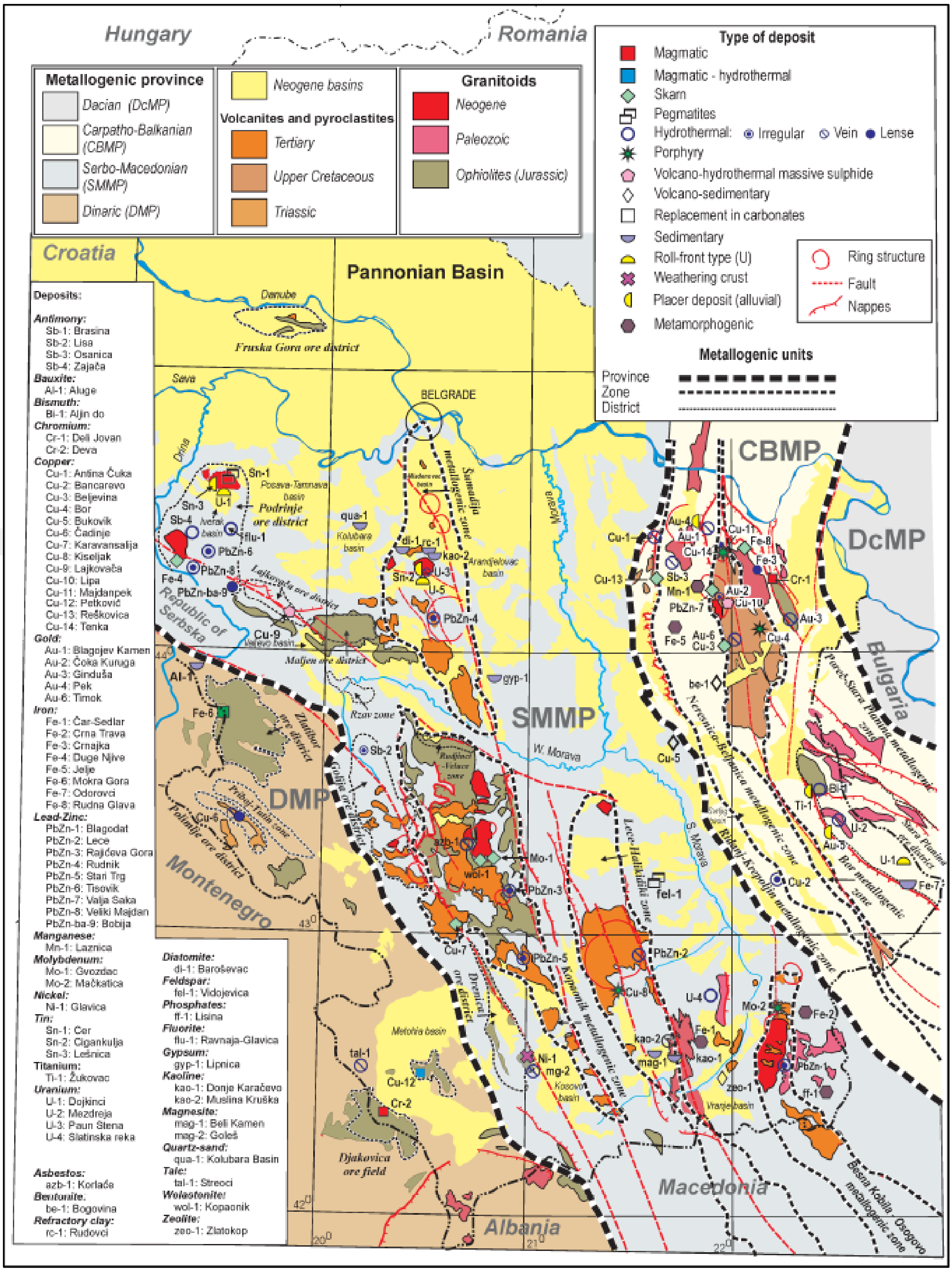

Figure 3.2 : The major metallogenic provinces and zones, mineral deposits and and industrial mineral occurrences of importance in Serbia. CBMP: Carpatho-Balkanian metallogenic province; DcMP: Dacian metallogenic province; SMMP: Serbo-Macedonian metallogenic province; DMP: Dinaric metallogenic province**.** The map has been taken from Jelenković et al., (2008).

Contingent on the actual knowledge of plate tectonics and of the geotectonic and metallogenic development of the terrain in Serbia, its mineral resources can be classified as: (1) Deposits related to intracontinental rifting; (2) Deposits related to ophiolite complexes; (3) Deposits of subduction related setting and (4) Deposits of continent-continent collision-related setting (Janković, 1990).

For the purpose of the study, the deposits of subduction related setting (subduction underneath the active continental margin; Cretaceous) shall be discussed in Chapter 3.3, since the Carpatho-Balkanian metallogenic province is in close connection with subduction processes in the area.

3.3 Geological Evolution of the Carpatho-Balkanian Metallogenic Province

Most deposits in the eastern Serbian part of the Carpatho-Balkanian metallogenic province are in correlation with horst-graben structures developed above subducted oceanic lithosphere under the Eurasian plate, after the closure of a Tethyan branch in the course of the Early Cretaceous (Janković, 1990).

The Carpatho–Balkan mountain chain is an eastern branch of the European Variscan orogeny, a belt ranging from the South Carpathians in Romania to the Black Sea in the eastern part of Bulgaria, encircles the western margin of the Moesian foreland Platform (Jovanović et al., 2019). In eastern Serbia and western Romania, Carpatho–Balkanides, a N–S to NNW–SSE, more than 200 km long belt spans further to the east to Bulgarian Balkan orogen and can also be observed southward, following the eastern rim of the Eastern Vardar Ophiolitic Unit, extending into Northern Greece (Schmid et al., 2008).

Tethys–Paratethys ocean controlled the tectonic evolution of the Carpatho–Balkanides in the Alpine period due to opening and closure processes (Janković, 1997) and Carpatho–Balkanides shaped around its current arrangement owing to Alpine tectonics (Gallhofer et al., 2015). For the subduction of ocean(s) and the convergent movement betwixt African and European plates drove the collision of continental blocks with the European continent, the Carpatho-Balkanian orogen ultimately came into its presence (Csontos and Vörös, 2004; Schmid et al., 2008).

Dimitrijević (1997) suggests that the geotectonic units of the Serbian part of Carpatho-Balkanides are divided into four major groups: Supragetic, Getic, Upper Danubian (Infragetic) and Lower Danubian (Table 3.1; Figure 3.3.b).

Table 3.1 : Geotectonic association of three sectors of the Carpathian–Balkanides with nomenclature of Alpine units and pre–Alpine basement (Haydoutov, 1989; Săndulescu, 1994; Kräutner and Krstić, 2003; Jovanović et al., 2019).

<table>
<tr><th colspan="2">Romanian South Carpathians</th><th colspan="2">East Serbian Carpatho–Balkanides</th><th colspan="2">Bulgarian Balkan Mountains</th></tr>
<tr><th>Alpine Unit</th><th>Pre–Alpine basement</th><th>Alpine Unit</th><th>Pre–Alpine basement</th><th>Alpine Unit</th><th>Pre–Alpine basement</th></tr>
<tr><td></td><td></td><td>Supragetic Serbo–Macedonian Massif</td><td></td><td></td><td>Morava unit</td></tr>
<tr><td>Median Dacides – Getic</td><td>Sebes–Lotru terrane (Ordovician, North African orogen, magmatic arc)</td><td>Getic</td><td>Kučaj terrane (Late Proterozoic to Early Cambrian volcanic arc)</td><td>Sredna Gora nappes</td><td>Iskar–Svoge</td></tr>
<tr><td rowspan="3">Marginal Dacides – Danubian</td><td>Tisovita (Devonian oceanic suture)</td><td>Upper Danubian</td><td>Stara Planina–Poreč terrane (Proterozoic to Neoproterozoic and Early–Mid Paleozoic; island arc + ophiolites)</td><td rowspan="3">Balkan nappes</td><td>Berkovica Group (island arc + ophiolites)</td></tr>
<tr><td>Dragsan terrane (Early Neoproterozoic, Avalonia)</td><td rowspan="2">Lower Danubian</td><td rowspan="2">Vrška Čuka–Miroč terrane (Neoproterozoic volcanic arc)</td><td rowspan="2">Late Proterozoic, Cadomian, Gondwana – derived</td></tr>
<tr><td>Lainici–Paius terrane (Neoproterozoic, Amazonian Cadomian)</td></tr>
</table>

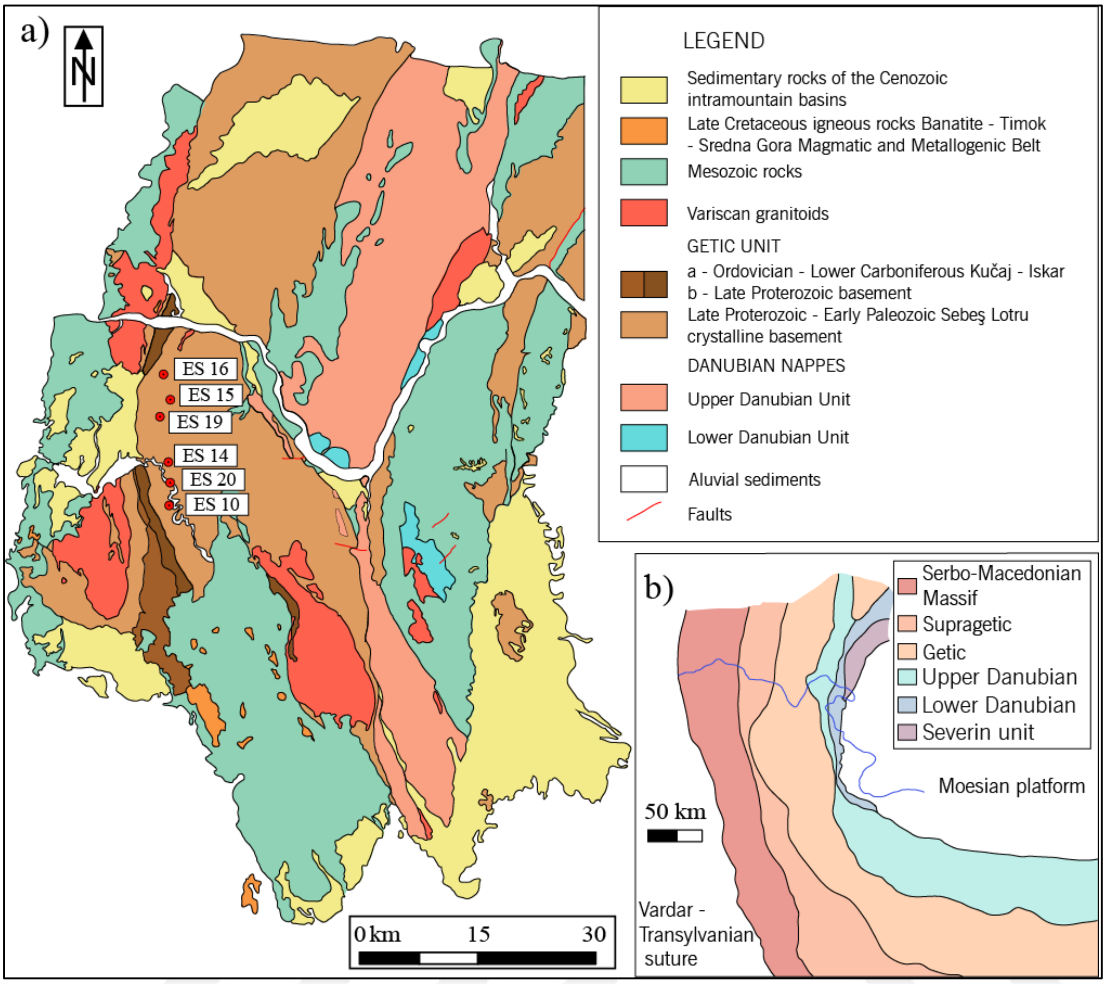

Figure 3.3 : a) Geological map of the targeted area with associated units (Kräutner and Krstić, 2003; Anzulović, 2022); b) a geotectonic outline of the Carpathian–Balkan sector (Krstić and Karamata, 1992; Karamata, 2006).

The basement of the Getic–Supragetic nappe sequence consists of medium to high grade Neoproterozoic to Early Paleozoic gneiss and Paleozoic greenschist to sub–greenschist metabasic rocks unconformably covered by Late Carboniferous to Permian fluvial sediments (Iancu et al., 2005), with detrital material stemmed from the European continent. The basement is also intruded by Variscan plutons that crop out at many places in Serbia and Bulgaria (Jovanović et al., 2019).

The Supragetic (highest structural level) unit comprises the Gornjak-Ravanica Zone (Silurian and Devonian sediments, Permian red sandstone and Mesozoic with numerous breaks in sedimentation). The basement is characterized by the system structurally on top (upthrusted sequence) of the Getic unit. Such arrangement prefers the Alpine structural style (overprint) instead of a main depositional pattern (Spahić et al., 2019). The Supragetic unit metamorphic basement includes sundry volcano–sedimentary rocks of Ordovician–Silurian protolith age (Krstekanić et al., 2017). They consist chiefly of low to intermediate–grade Proterozoic and Paleozoic rocks (Karamata, 2006). These units extend into Western Bulgaria, where they are renowned for the "Morava Unit" and constitute the upper plate of the Osogovo–Lisets core complex (Kounov et al., 2004; Schmid et al., 2008).

The Getic represents a large-scale tectonic zone in the Alpine tectonic framework of the Carpatho-Balkan orogen, including a number of tectonic units forming southeast-, east- and northeast- vergent nappes and makes up the Ruj Zone (Upper Jurassic Flysch), Suva Planina Zone (Devonian—Lower Carboniferous Flysch, Permian sandstone, thick Jurassic and Cretaceous carbonates), Kučaj Zone (clastics from Cambrian to Devonian, flysch, Permian and Triassic clastics, Jurassic-Lower Cretaceous carbonates, thin Upper Cretaceous), Timok Eruptive Area, and the Tupižnica-Tepoš unit (Mesozoic carbonates with frequent breaks).

The Upper Danubian and Lower Danubian are thrusted over the stable Moesian Platform and are structurally in a lower position with respect to the Getic unit. The Stara Planina–Poreč Unit can be correlated with the Devonian oceanic suture zone Tisovita terrane in the South Carpathians (Balintoni et al., 2014) and Berkovica group (Yanev, 2000). The Upper Danubian consists of the Poreč Zone (fairly complicated relations of Cambrian to Aptian rocks; Deli Jovan Gabbro), Miroč Zone (partly the entire Paleozoic; Jurassic and Cretaceous differing in thickness, with breaks); Krajina Zone (Sinaia Beds, Mokranje Flysch) and the Stara Planina (semi-metamorphic Paleozoic, Permian red sandstone, Mesozoic up to the Cretaceous; Zaglavak Gabbro; granitoids of distinct ages). The Lower Danubian unit is representative of the Vrška Čuka Zone (Cambrian? greenschists, relatively thin Carboniferous and Permian, thin Jurassic and Cretaceous).

Jelenković et al. (2002) proposes that the metallic mineral deposits of the Carpatho-Balkanian metallogenic province are grouped into a few metallogenic zones with exact associations of elements and genesis: Ridanj-Krepoljina, Neresnica-Beljanica, where study area of the thesis is located, Bor and Porec-Stara Planina metallogenic zones (Figure 3.4). The occurrence of the above mentioned deposits have been related to various geologic settings and processes, in which of specific economic significance are Cu-Au ± Pb-Zn deposits linked to the processes of intracontinental rifting and associated magmatic activity in the region of Bor metallogenic zone, and deep rift structures across the subduction zone in the area of the Ridanj-Krepoljina.

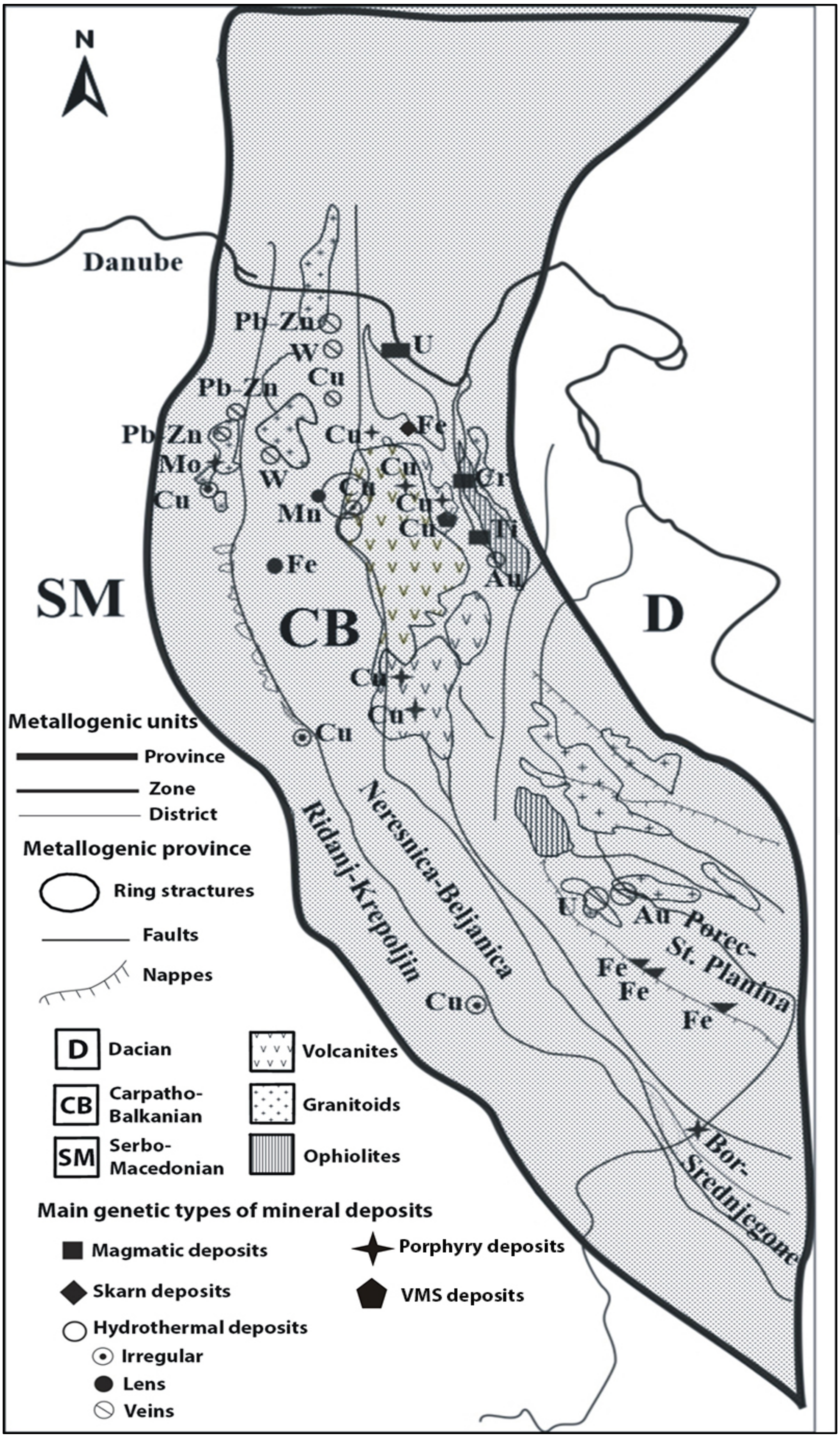

Figure 3.4 : A detailed map of the Carpatho-Balkanian metallogenic province – Eastern Serbia Sector (modified after Jelenković et al., 2002).

4. PETROGRAPY

4.1. General Mineralogy

According to the diffractogram shown in Figure 4.1, pargasite, dravite, epidote, anorthite and chlorite shows could be interpreted as inclination towards a mafic type of an igneous source. X-ray diffractograms of the other samples demonstrated quartz, plagioclase, calcite and amphibole minerals being the most abundant, also while including tremolite, montmorillonite, muscovite, epidote, clinochlore, phylogopite, pargasite and ferropargasite minerals. The intensities of X-ray peaks for dominant minerals such as quartz and plagioclase in each analysis get amplified due to decrease in grain size.
Another XRD analysis that was conducted on the sample T10-D at the XRD laboratory of the Faculty of Istanbul Technical University gave away a particular manganese dioxide mineral of pyrolusite in the XRD profile as follows below (Figure 4.2).

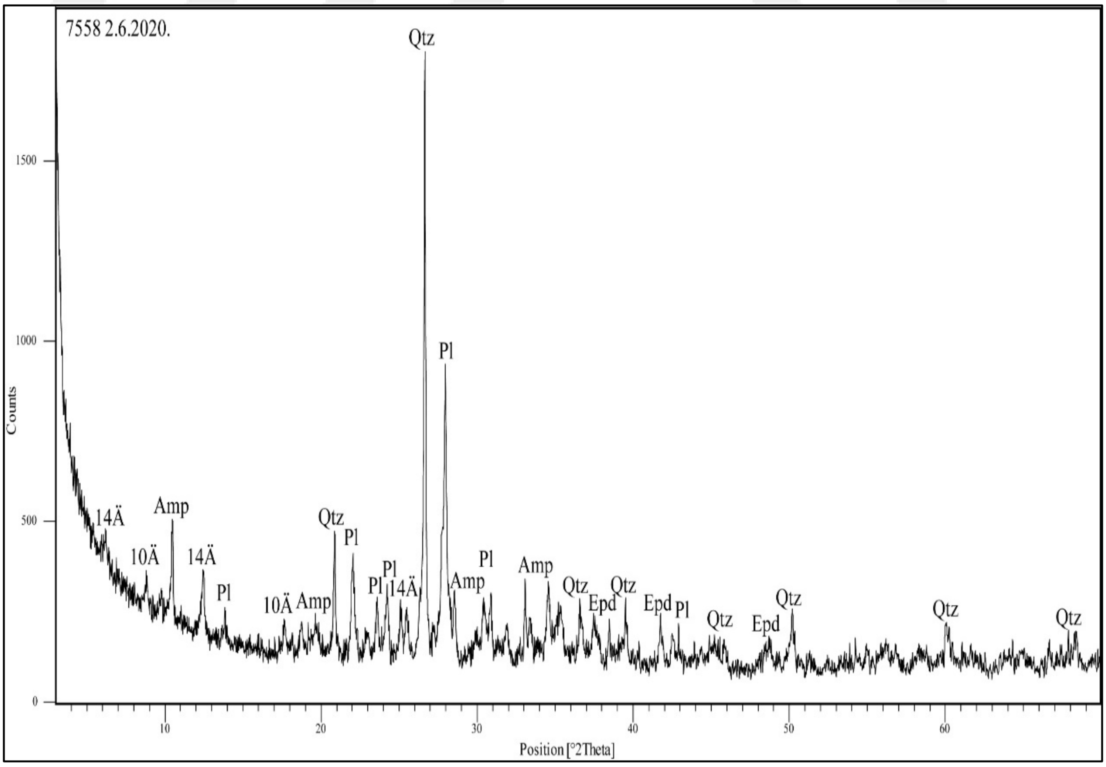

Figure 4.1 : X-ray diffractogram of sample 7558 (Amp: Amphibole; Qtz: Quartz; Pl: Plagioclase; Epd: Epidote).

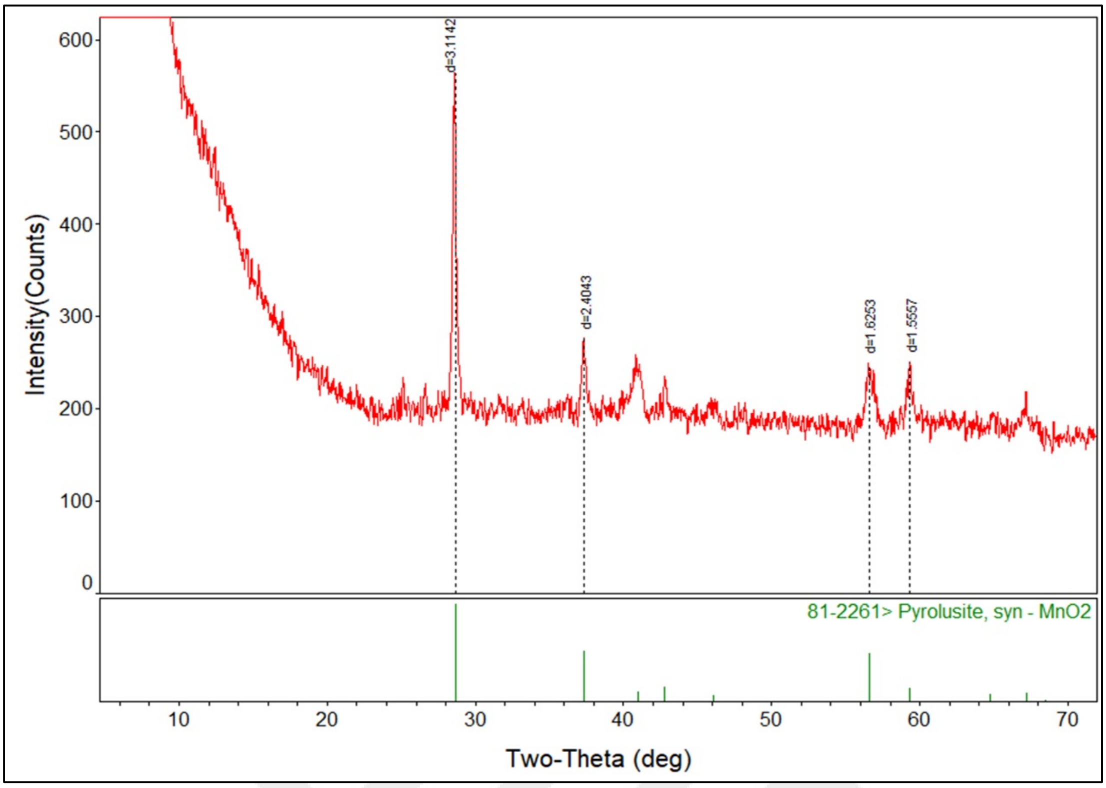

Figure 4.2 : XRD spectrum of the metallic phase concentrated in the sample T-10D yielding manganese dioxide mineral of pyrolusite.

For study purposes, sixteen different hand specimens that could have high probabilities of ore-markings and important indications were brought from the study area to be investigated at the laboratories of Istanbul Techincal University. These hand specimens were carefully chipped and prepared as both polished and polished thin sections by an experienced lab technician of the faculty.

The polished thin sections were then looked upon under optical microscope in order to compare and match the formerly obtained XRD results and this comparison successfully showed identical findings. While quartz, feldspar and muscovite being the most copious, garnet, sericite, sphene (titanite), actinolite, glaucophane (?), plagioclase, chlorite and biotite minerals were also detected in almost each sample. The samples at hand were accordingly subclassified into quartz-muscovite-chlorite-garnet schists. Highly altered needle-like muscovite and feldspar minerals observed in certain samples explain the presence of sericite and tell us about the sericitation (phyllic alteration) despite not being very common (Figure 4.3.a). The quartz are at times seen pinched together as huge clusters due to palpable metamorphism and schistosity (Figure 4.3.b).

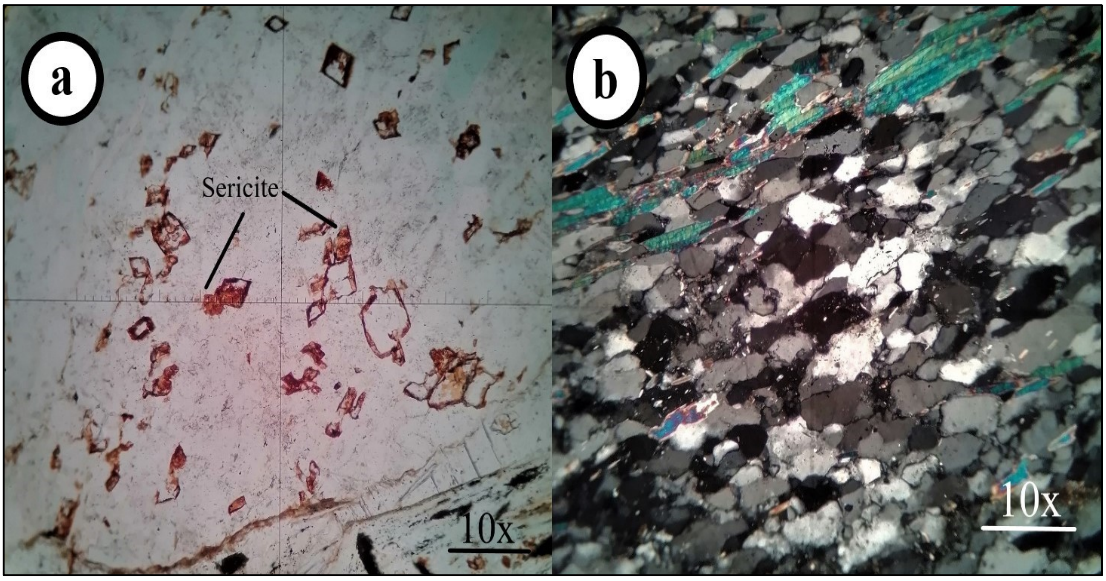

Figure 4.3 : Photomicrographs illustrating certain characteristics of the minerals**.** a) Traces of serizitation in sample T10-F2 taken in plane polarized light; b) clenched quartz minerals that show foliation habit in sample T15-B5 taken under crossed polars.

Anzulović (2022) proposes that the select metamorphic units of the prospection area belong to the green schist and amphibolite facies with a continual increase of pressure and temperature factors illustrated in the P-T plot (Figure 4.4), adding that these values show an escalation towards the southeast of the Blagojev Kamen vicinity (Figure 4.5).

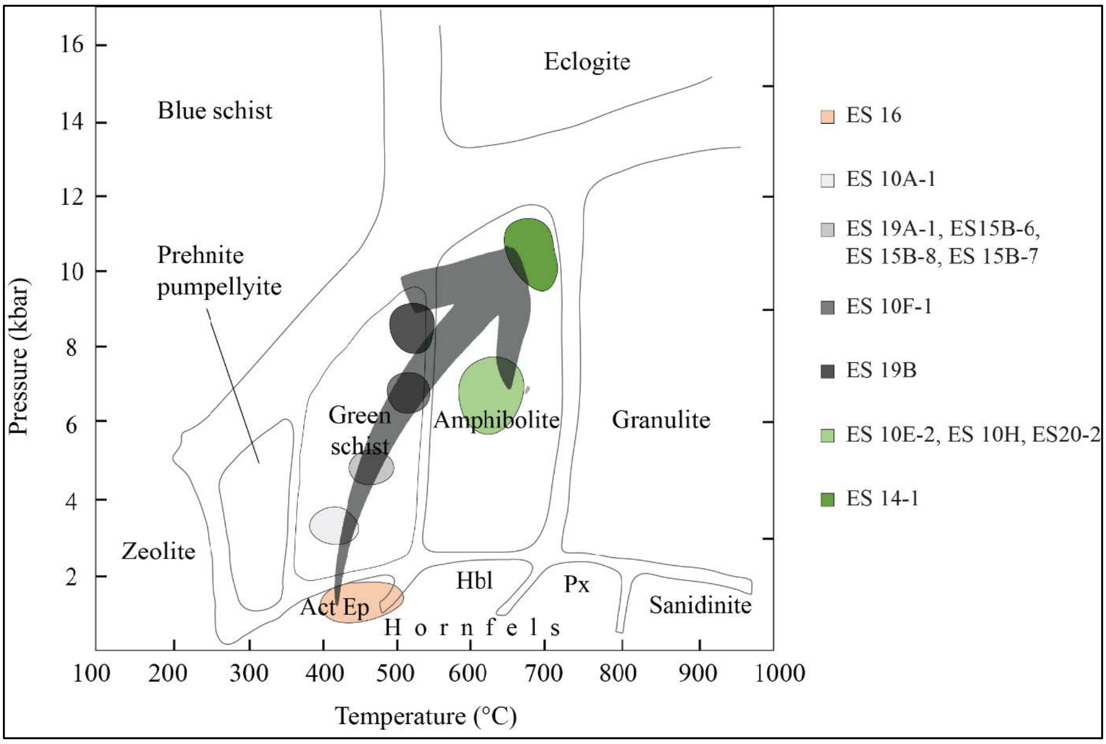

Figure 4.4 : P-T diagram of the prospected samples and their relevant facies groups (Anzulović, 2022).

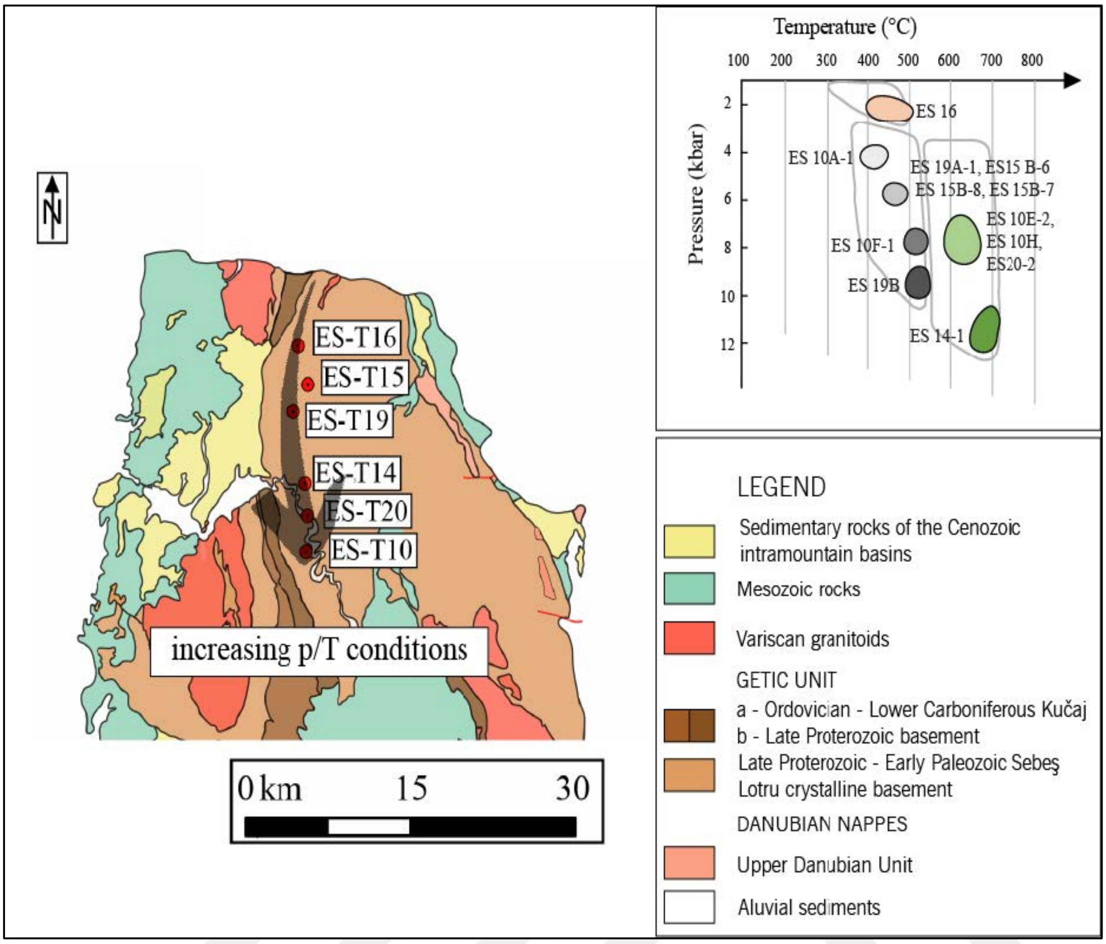

Figure 4.5 : Geological map of the select samples based on their facies groups. The arrow signifies an increase in the pressure and temperature conditions southward for the metamorphic facies (Anzulović, 2022).

4.2 Ore Mineralogy

Of all the ore minerals encountered in the polished sections under ore microscope, pyrite comes as the most common followed by chalcopyrite, goethite, sphalerite, ilmenite (?) and pyrolusite, respectively. The pyrite and chalcopyrite are of an epigenetic nature whereas the pyrolusite seems to have syngenetic (?) occurrence. The variety of ore minerals is only limited to some extent since the hand specimens were explicitly obtained from wall rock boundaries, or else the residual rocks that had been left after the mining exploitation in the 1960s could address the situation itself.

Pyrite is majorly present in each polished section ranging from euhedral to subhedral forms and its perfect cubic structure can be observed in many (Figure 4.6.f). It also assimilates a dissemination pattern throughtout the sections of green schist (Figure 4.6.h), albeit in quite small to moderate sizes and in a rather oxidized state while still remaining fresh in many occasions. However, in one of the sections of quartz vein, the pyrite manifests a cataclastic texture with visible deformation and fills in cavities and fractures, which might eventually point out to a series of post-formational tectonic activities in the area (Figure 4.6.a). Judging from the replacement of the pyrite by goethite in section T15-B5, it can be inferred that the high oxidation stage had led to goethitization over a vast period of time (Figure 4.6.b). In addition, the pyrite in one of the polished sections occupies the cavities of the calcite vein cross-cutting quartz minerals.

Chalcopyrite is the second most common ore mineral in the sections and is mainly a replacement product of pyrite. It is also in association with sphalerite and goethite in other observations. In many cases, chalcopyrite is seen to have been replaced by goethite and on the other hand, indicate to either have formed as inclusions in pyrite and quartz or have sealed along the fractures and cavities owing to post-reactions with sulfide in the system (Figure 4.6.c, g). This, hence, holds true that the mineralization of the pyrite had occurred prior to that of chalcopyrite.

Sphalerite has been merely seen in the polished section of the sample T10-E2 as a replacement product within the pyrite alongside the peculiar boundaries with the chalcopyrite. It is understood from the intact rims between the chalcopyrite and sphalerite that these two minerals might have crystallized on the near-simultaneous time threshold meanwhile the pyrite had formed primarily in the paragenetic sequence (Figure 4.6.d). Based upon the metallogenic map of Serbia (Jelenković et al., 2008), the presence of Pb could be linked to the potential contamination from the granitoid intrusions close to the sampling locations in the proximity.

Pyrolusite has a very brittle fibre, which is considerably prone to breaking, and a metallic lustre with pitch-black colour in its pure form. The syngenetic (?) occurrence of the pyrolusite (MnO_2) in the sample T10-D, which can clearly be noticed as distributions throughout the section in elongated subhedral forms with bluish steel gray colour and matte lustre (Figure 4.6.e), hints that it could have been introduced foremost to the ore system in veins with quartz and other metallic minerals by the alteration of manganite ($MnO(OH)$), rutile (TiO_2) and/or sphene ($CaTiSiO_5$) from the rock complex. The mechanism behind the alteration must have been driven by extreme weathering conditions in shallow marine environments or by circulating meteoric water (Parker, 2017).

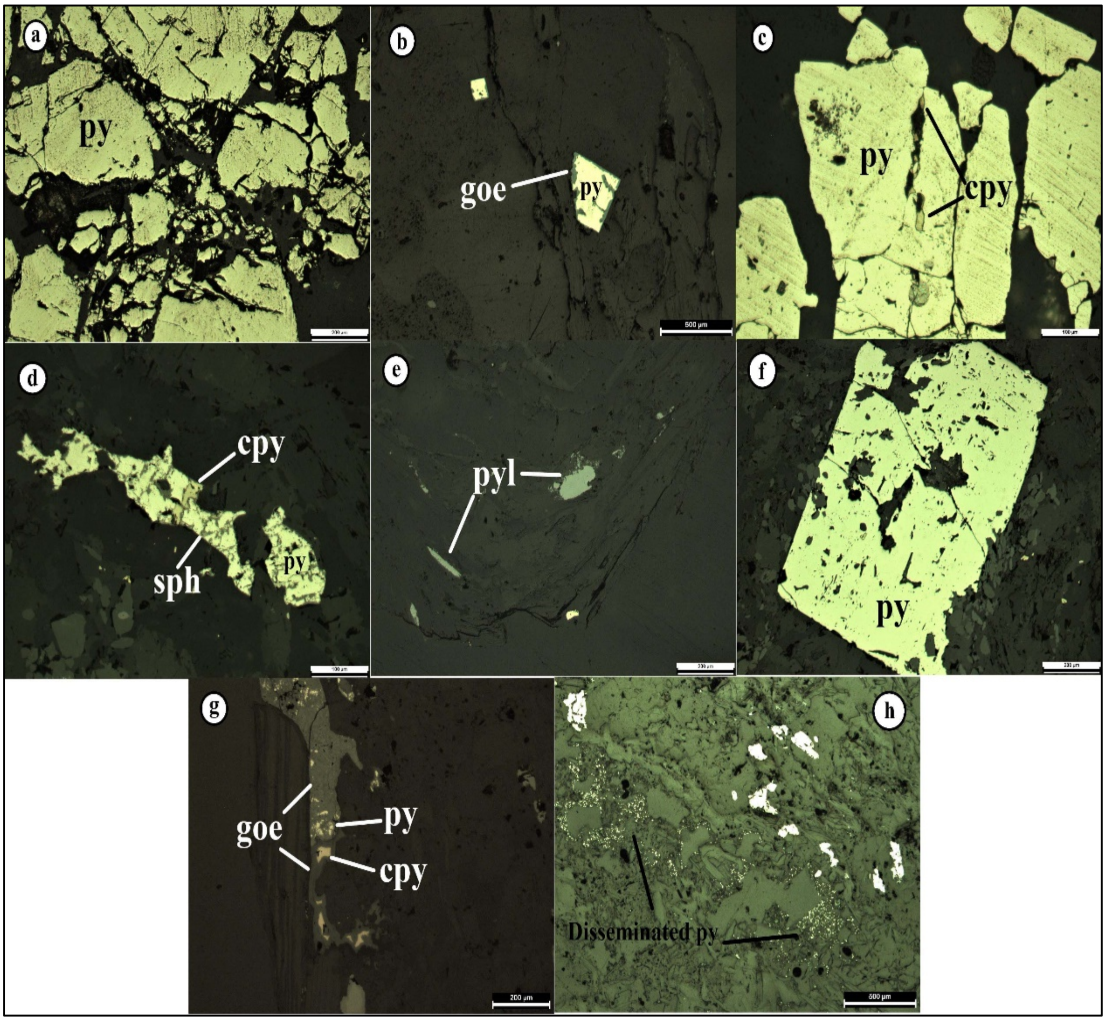

Figure 4.6 : Photomicrographs of ore minerals demonstrating indicative replacement examples and textures. a) Granular pyrite minerals with fragmental cataclastic texture (ppl); b) goethite mineral replacing pyrite (ppl); c) secondary minor chalcopyrite inclusions in pyrite (ppl); d) sphalerite replaces pyrite, co-existing with chalcopyrite (ppl); e) pyrolusite minerals that developed in accordance with formation of host rock (ppl); f) greatly altered massive pyrite mineral in cubic form (ppl); g) goethite replacing both pyrite and chalcopyrite to a large extent (xpl); h) respectably small pyrite occurrences in dissemination patterns (ppl). Abbreviations: Py – pyrite, cpy – chalcopyrite, goe – goethite, sph – sphalerite, pyl – pyrolusite.

4.3 Mineral Geochemistry

According to the data obtained from the analyses, the average values of each sample correspond to a very small amount of concentration for trace elements. Mn shows the hightest average value (1052.87 ppm/0.105 wt.%) while W averages only 9.28 ppm (0.000928 wt.%) and no trace of Au was detected in the analysis.

Table 4.1 : ICP-MS analysis results for major and trace elements of the Blagojev Kamen deposit (ppm).

Sample	Mn	Ni	Cr	Zn	Pb	Cu	Co
T10A-1	837	283.6	214	42	14.9	14.4	17
10F-1	947	163.2	363	92	4.4	14.5	52.2
15B-6	1050	191.4	305	67	10.3	1.7	38.8
15B-8	1609	308.2	258	163	6	26.9	47.4
15C-1	1350	1198.1	455	172	505.1	18.1	4.4
T16	1211	375.1	380	116	6.1	39.2	46.1
T19A-1	608	693.6	333	93	12.8	9	13.6
T19B	811	624.8	306	99	12.5	130.1	25.5
Average	1052.87	479.75	326.75	105.5	71.51	31.73	30.72

Table 4.1 (Continued) : ICP-MS analysis results for major and trace elements of the Blagojev Kamen deposit (ppm).

Sample	Ta	W	Sn	Mo	Ag	Au
T10A-1	0.7	7	<5	2.28	0.12	N/A
10F-1	0.8	41	<5	0.78	0.1	N/A
15B-6	0.7	1	<5	0.85	0.05	N/A
15B-8	1	2	<5	1.45	0.09	N/A
15C-1	0.5	5	<5	2.48	0.34	N/A
T16	1.3	<1	<5	1.07	0.17	N/A
T19A-1	0.8	6	<5	1.25	0.08	N/A
T19B	0.9	3	<5	6.78	0.18	N/A
Average	9.3	9.28	<5	2.11	0.14	N/A

Table 4.2 : ICP-AES analysis results for oxide minerals of the Blagojev Kamen deposit (wt. %).

Sample	SiO_2	TiO_2	Al_2O_3	Fe_2O_3	Cr_2O_3	CaO
T10A-1	53.62	1.1	14.03	7.46	0.03	8.43
10F-1	35.61	2.49	19.06	12.45	0.05	8.09
15B-6	44.77	1.73	15.68	7	0.04	10.56
15B-8	41.82	2.34	13.97	12.62	0.03	8.59
15C-1	74.44	0.19	2.76	4.15	0.06	7.75
T16	48.86	2.43	14.65	11.26	0.05	9.17
T19A-1	65.77	0.65	12.46	5.37	0.04	2.87
T19B	60.06	0.82	15.77	7.49	0.04	1.57
Average	53.12	0.18	1.69	1.06	0.01	0.89

Table 4.2 (Continued) : ICP-AES analysis results for oxide minerals of the Blagojev Kamen deposit (wt. %).

Sample	CaO	MgO	MnO	K_2O	Na_2O	P_2O_5
T10A-1	8.43	2.04	0.11	3.17	1.11	0.17
10F-1	8.09	7.22	0.13	3.62	0.13	0.23
15B-6	10.56	3.65	0.13	1.07	4.06	0.32
15B-8	8.59	7.77	0.21	0.46	1.69	0.37
15C-1	7.75	0.74	0.16	0.78	0.03	0.05
T16	9.17	6.54	0.15	0.76	2.16	0.35
T19A-1	2.87	2.32	0.07	1.45	2.87	0.16
T19B	1.57	2.91	0.1	2.54	2.62	0.16
Average	0.89	0.52	0.02	0.22	0.23	0.03

Table 4.3 : ICP-MS analysis results for REE of the Blagojev Kamen deposit (ppm).

Sample	Ce	Y	Sc	Nd	La	Dy	Pr	Gd	Sm
T10A-1	44.8	31	25	23.7	20.8	5.28	5.7	5.51	5.55
10F-1	20.7	41.3	44	14.5	7.7	6.93	3.01	5.02	3.91
15B-6	16.3	26.7	42	11.7	6.6	4.67	2.48	3.87	3.37
15B-8	38.7	22	25	21.1	17.8	4.16	5.06	4.48	4.67
15C-1	11.1	13.4	4.3	5.9	5.3	2.22	1.47	1.71	1.48
T16	45.9	24.9	32	24.7	21.9	4.94	5.99	5.43	5.4
T19A-1	37.5	20.6	16	18.1	18	3.54	4.7	3.64	3.83
T19B	69.1	30.4	21	31.7	33.1	5.74	8.36	5.87	6.7
Average	35.5	26	26	18.9	16.4	4.69	4.6	4.44	4.36

Table 4.3 (Continued) : ICP-MS analysis results for REEs of the Blagojev Kamen deposit (ppm).

Sample	Th	Er	Yb	U	Eu	Ho	Tb	Tm	Lu
T10A-1	4.3	2.91	2.77	1	1.4	1.04	0.91	0.44	0.47
10F-1	0.4	4.19	3.72	1	1.17	1.42	0.94	0.63	0.58
15B-6	0.7	2.67	2.5	0.9	1.21	0.94	0.69	0.4	0.39
15B-8	1.8	2.28	2.05	1	1.25	0.78	0.68	0.34	0.34
15C-1	1.2	1.31	1.18	0.5	0.65	0.42	0.31	0.19	0.17
T16	2.4	2.49	2.02	2	1.79	0.9	0.82	0.34	N/A
T19A-1	4.4	2.09	1.97	0.9	0.93	0.7	0.55	0.31	0.3
T19B	9.1	3.61	3.45	3.3	1.55	1.14	0.97	0.51	0.51
Average	3	2.69	2.46	1.3	1.24	0.92	0.73	0.4	0.39

5. STABLE ISOTOPE ANALYSES

5.1. Sulfur Isotope Analysis

For the purpose of isotopic determination of the sulfur entity in the Blagojev Kamen deposit, pieces of pyrite collected from a schist hand specimen that bear the most pyrite in quantity have been used for $\delta^{34}S$ analysis. This hand specimen was recovered from an outcrop due south of the Blagojev Kamen village by the Pek River. The analysis could be only run on a single pyrite sample due to shortness of amount and variety of the sulfide minerals available in the hand specimens. Analysis results revealed that the average value for $\delta^{34}S$ corresponds to +2.15‰ as shown in Table 5.1.

Table 5.1 : $\delta^{34}S$ values for the sulfide minerals of the Blagojev Kamen deposit. Abbreviations: Py – pyrite.

Sample ID	$\delta^{34}S$ (‰)
T10-E2 - py	2.3
T10-E2 - py (repetition)	2.0
Average	2.15

According to the statement of Hoefs (1987), on condition that the deposits whose $\delta^{34}S$ values are close to the zero boundary ought to be interpreted as a sulfur source of igneous origin, both sulfur libareted from magmas and sulfur precipitated from sulfides in igneous rocks combined. Based on this hypothesis, the source of sulfur belonging to the Blagojev Kamen deposit must have derived from an igneous source (Figure 5.1).

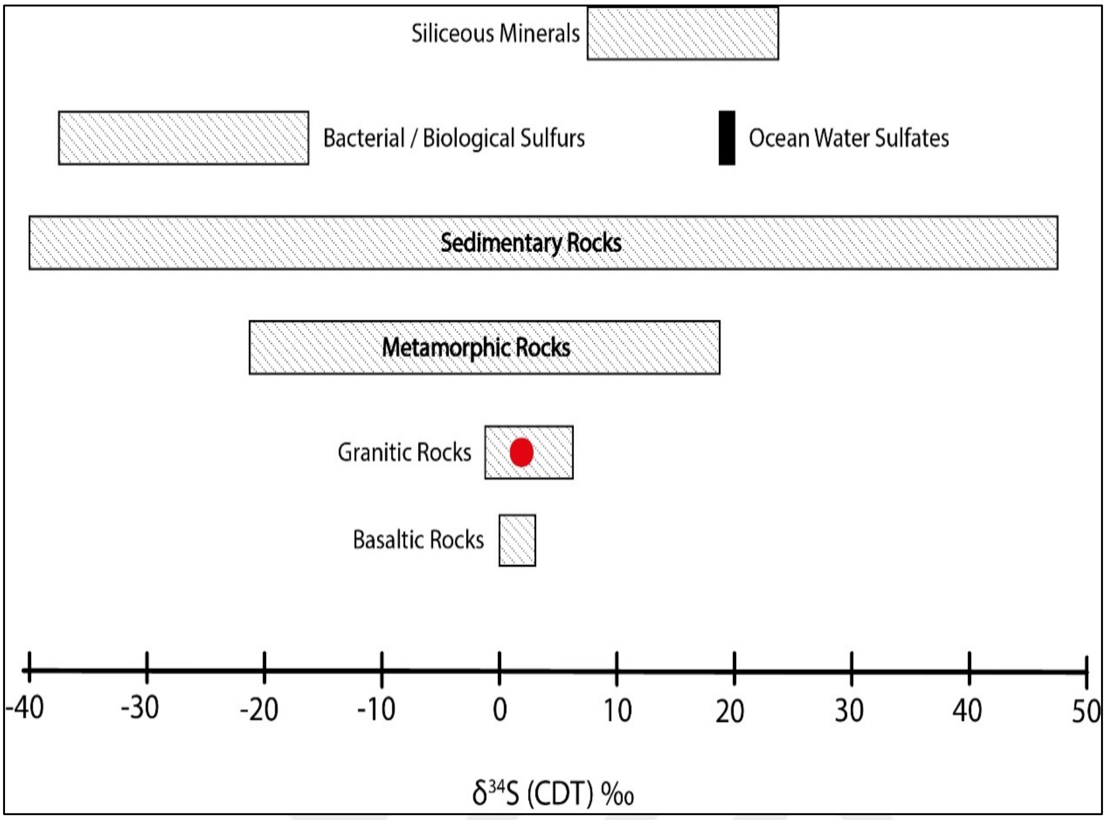

Figure 5.1 : Sulfur isotope compounds of certain geologically significant metarials. The red dot coincides with the sulfur isotope value for the Blagojev Kamen deposit (modified after Hoefs, 1987).

5.2 Oxygen Isotope Analysis

The identification of the $\delta^{18}O$/ $\delta^{16}O$ isotope values and the temperature estimations attained from oxygen bearing minerals can also give us clues on the type of fluid generation. These temperature values can be achieved with the help of fluid inclusion studies.

So as to unveil the fluid properties, select quartz minerals from the most quartz-rich hand specimen (greenschist) have been used for $\delta^{18}O$ analysis. After the collection of the said quartz minerals under the stereo microscope, HCl acid solution was applied to cleanse them of unwanted carbonates and any other materials.

Double-run analysis results showed that the VSMOW $\delta^{18}O$ values of +11.5 and +11.7‰, averaging +11.6‰ (Table 5.2). With the aim of calculating the $\delta^{18}O_{water}$ content in the quartz sample, a formula given by Sharp and Kirschner (1994) have been taken as a reference:

$$10^3 \ln \alpha^{quartz}_{water} = \frac{3.38 \times 10^6}{T^2} - 3.4 \approx \Delta^{quartz}_{water} = \delta^{18}O_{quartz} - \delta^{18}O_{water} \quad (5.1)$$

,where T factor (in Kelvin) is determined by the average homogenization temperature of the fluid inclusions in the quartz samples. In this respect, T variable corresponds to 253 °C/536 K. In order for δD_{water} values to be found, the resulting $\delta^{18}O_{water}$ values from Equation 5.1 have been utilized in the following formula proposed by Craig (1961):

$$\delta D_{water} = 8 \times \delta^{18}O + 10 \quad (5.2)$$

Consequently, both $\delta^{18}O_{water}$ and δD_{water} outputs from the calculations are given in Table 5.2.

Taylor (1974) expresses that $\delta^{18}O$ values being in a wide range of +5 to + 25‰ and δD on -20 to -65‰ scale can be attributed to regional metamorphic waters (Figure 5.2; Figure 5.3), adding that rocks such as sandstones, greywackes, arkoses and volcanogenic sediments are most likely to contain low $\delta^{18}O$ values (δ = +8 to +13‰) owing that these sedimentary rocks generally preserve their initial $\delta^{18}O$ values through metamorphism.

Table 5.2 : $\delta^{18}O$ VSMOW values for the quartz minerals of the Blagojev Kamen deposit along with the calculated $\delta^{18}O_{water}$ and δD_{water} factors. Abbreviations: Qtz – quartz.

Sample ID	$\delta^{18}O$ VSMOW (‰)	$\delta^{18}O_{water}$ (‰)	δD_{water} (‰)
T15-B2 - qtz	11.50	3.14	35.12
T15-B2 - qtz (repetition)	11.70	3.34	36.72
Average	11.60	3.24	35.92

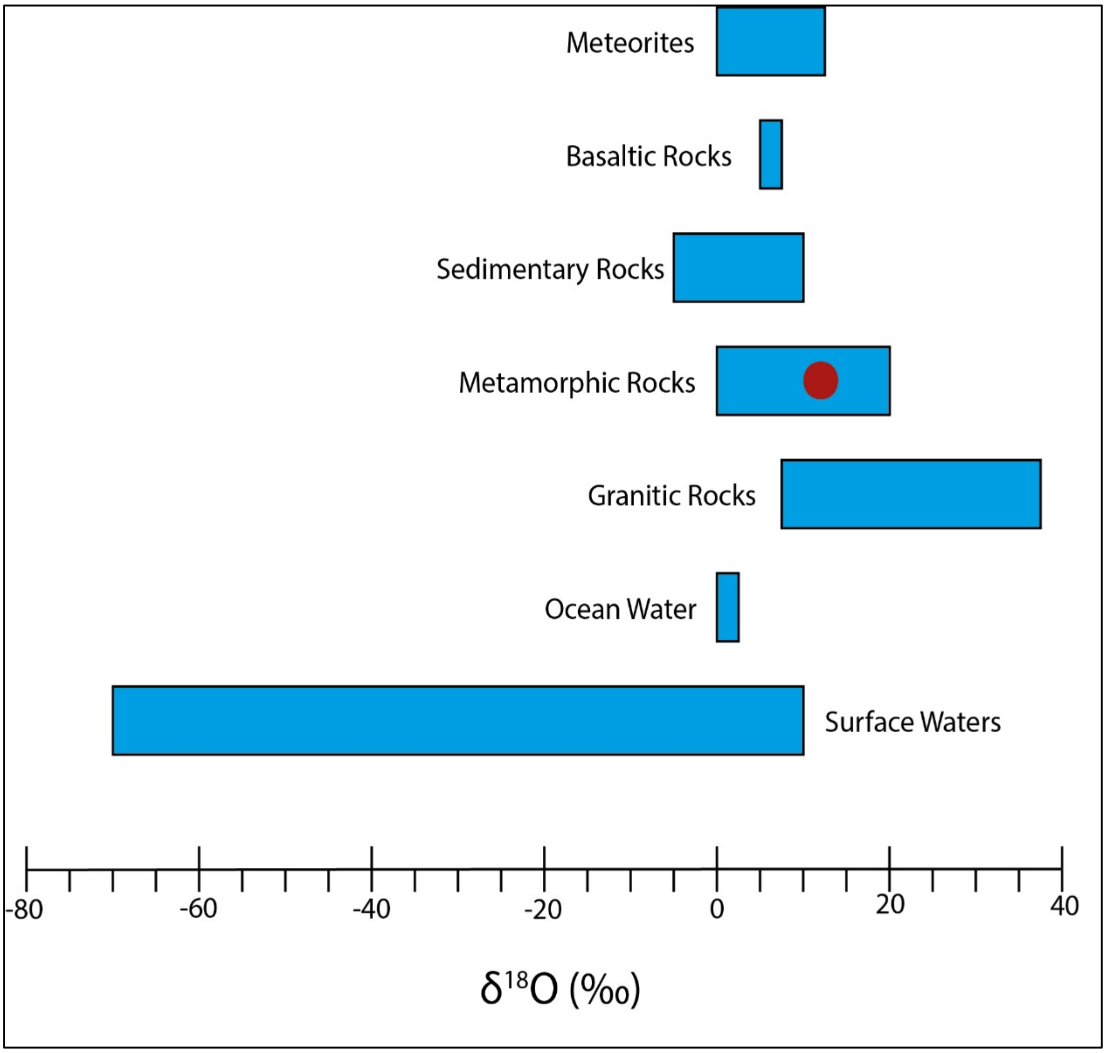

Figure 5.2 : $^{18}O/^{16}O$ ratios corresponding to specific oxygen-bearing materials based upon SMOW. The red dot marks the oxygen isotope value for the Blagojev Kamen deposit (modified after Hoefs, 1987).

Hydrothermal fluids that precipitate gold-containing quartz veins also correlate with the classification of metamorphic waters, which mostly turn out to be hefty and have differing values between +8 and +14‰ for $\delta^{18}O$ while it is -10 and -50‰ for δD. In addition, these fluids arguably tend to acquire their attributes from deep crustal origins (Hoefs, 1987).

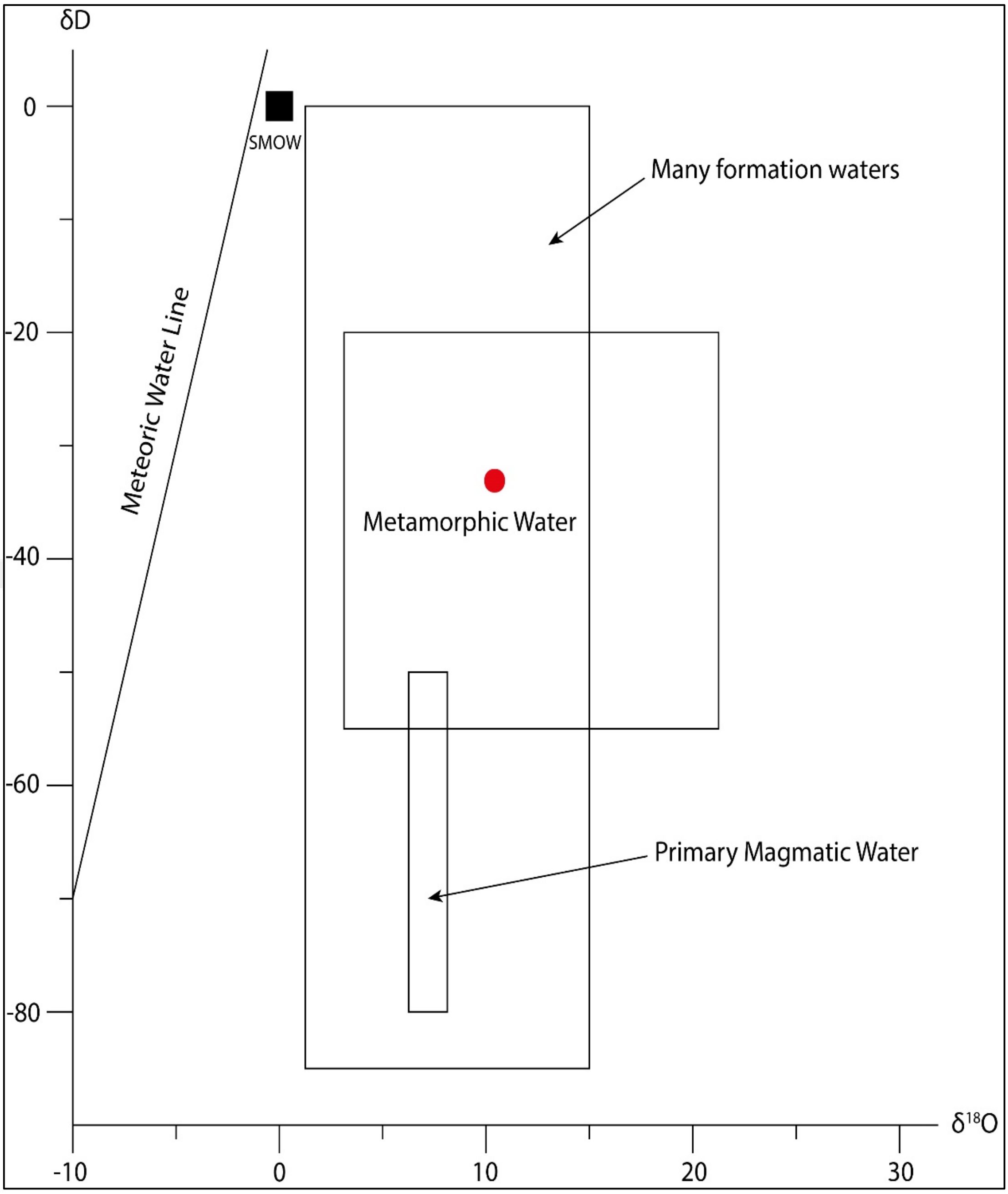

Figure 5.3 : δD versus δ^{18}O diagram for waters that are of diverse sources. The red dot illustrates the area to which the values belonging to the Blagojev Kamen deposit correspond (modified after Hoefs, 1987).

6. FLUID INCLUSION STUDIES

6.1 Petrography

Besides showing both primary and secondary inclusions within, all the samples predominantly presented quite small ones in size (~5-6µm), too (Figure 6.1). Eutectic/first melting (T_e), final melting (T_m) and homogenization (T_h) temperatures of these inclusions have been primarily evaluated during the analyses by initially cooling down the system to -100 ºC , followed by a heating process at a steady pace. The inclusions did mainly enclose either two-phase vapour (V) and liquid (L) or monophase liquid. L/V ratio of the inclusions falls in a broad percentage range between 20 and 80.

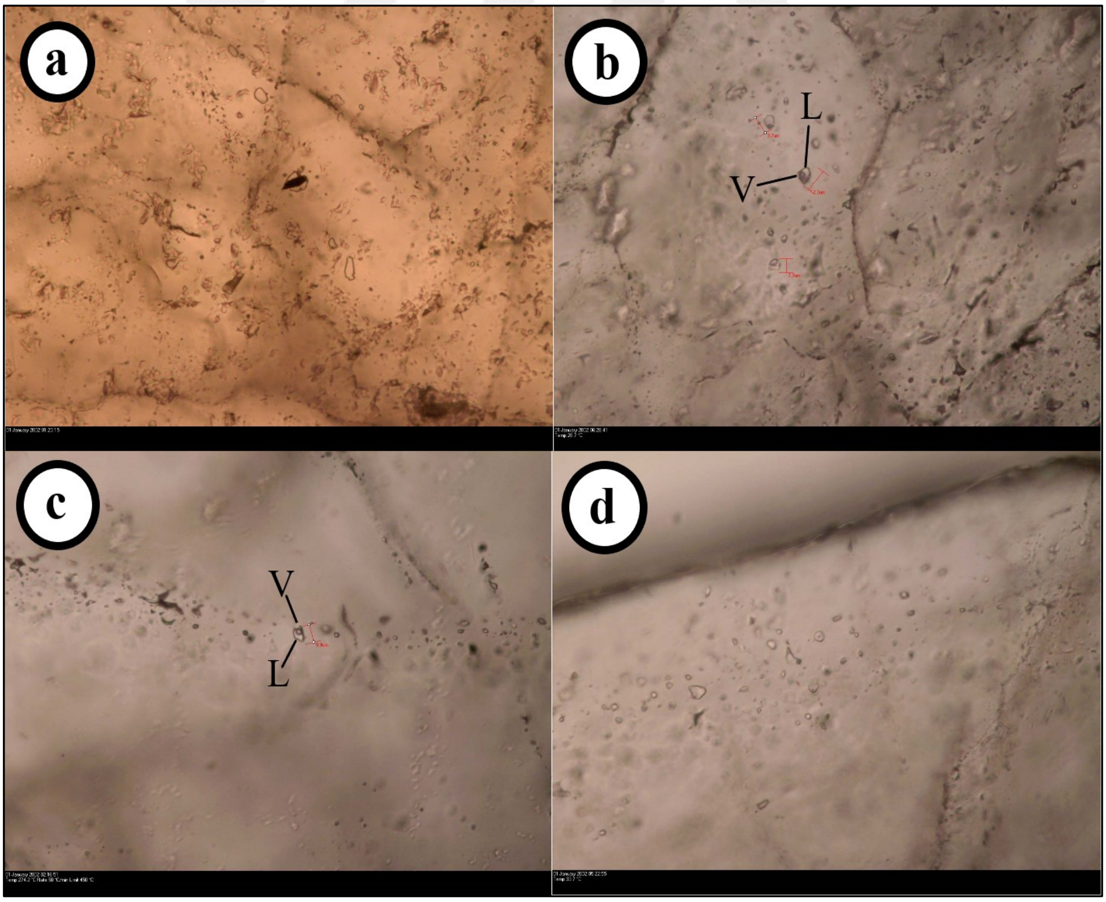

Figure 6.1 : Photomicrographs of the fluid inclusions spotted in the doubly-polished wafers. a) Single-phase liquid inclusions; b) and c) pseudosecondary two-phase (L+V) inclusions; d) secondary two-phase (L+V) inclusions.

6.2 Microthermometry

In total, eighty seven microthermometric measurements have been made on five different quartz minerals on the basis of T_e, T_m and T_h temperature parameters, a very small amount of which seemed to be primary inclusions and the rest is pseudosecondary and secondary inclusions only. Thus, the temperature factors of each inclusion have been taken notice in this study to be able to assess the T_h versus salinity values of the inclusions.

The measurement results for all said temperature types are as follows: Min: -56.5 ºC, Max: -34.7 ºC for the eutectic temperature; Min: -9.4 ºC, Max: -1.5 ºC for the last melting temperature; and Min: +186.1 ºC, Max: +390.3 ºC for the homogenization temperature. Also, it has been clearly noted that the homogenization temperature is for one of the inclusions is +236.6 ºC and the last melting temperature (clathrate) of the same inclusion was measured to be +7.94 ºC, which might be indicative of a carbonic gas mixture ($CO_2/CH_4/N_2$) inferring from the last melting temperature being much higher than the 0 ºC threshold value. Additionally, all the L+V inclusions showed to homogenize to the aqueous state when heated.

6.3 Fluid Salinity Content

Based upon the Bodnar (1993) equation, salinity content of the primary inclusions have been calculated and displayed in T_h-salinity diagram (Figure 6.2) and the frequency diagram is presented in Fiure 6.3. The consequent values appeared to be in the 2.57 – 13.29 equiv. wt.% NaCl array, only two of which amount to more than 10 equiv. wt.% NaCl while the rest relatively corresponds to low salinity content.

Although some pseudosecondary and secondary inclusions observed in the last quartz sample have not been included in the diagrams, it should still be remarked upon that these inclusions have high chances of contaning CO_2-clathrate, judging by their last melting temperatures that are above 0 ºC (predominantly ~ 8-9 ºC) . The CO_2 existence is most probably associated either with decarbonization reactions or oxidation process of the diffused hydrocarbons throughout the time of metamorphism (Higgins, 1980).

Higgins (1980) also denotes that the high quantities of CO_2 gas in the system is usually held accountable for the deposition of tungsten at high pressures and temperatures, all the while the pressure and temperature decreases happening in the CO_2 accelerate the deposition process even furher. Accordingly, this event should have contributed to the migration and concentration of tungsten with the help of carbonate/bicarbonate composites in the Blagojev Kamen deposit.

Despite the fact that some carbonic phases ($CO_2/CH_4/N_2$) in these inclusions have been traced at room temperature, there is also a minor amount of dissolved CO_2 gas in the solutions. The salinity estimations have been put forward according to the equation from Darling (1991) by taking the last melting temperatures of the clathrate (T_m (Cla) between 0 and + 10 ºC) into consideration.

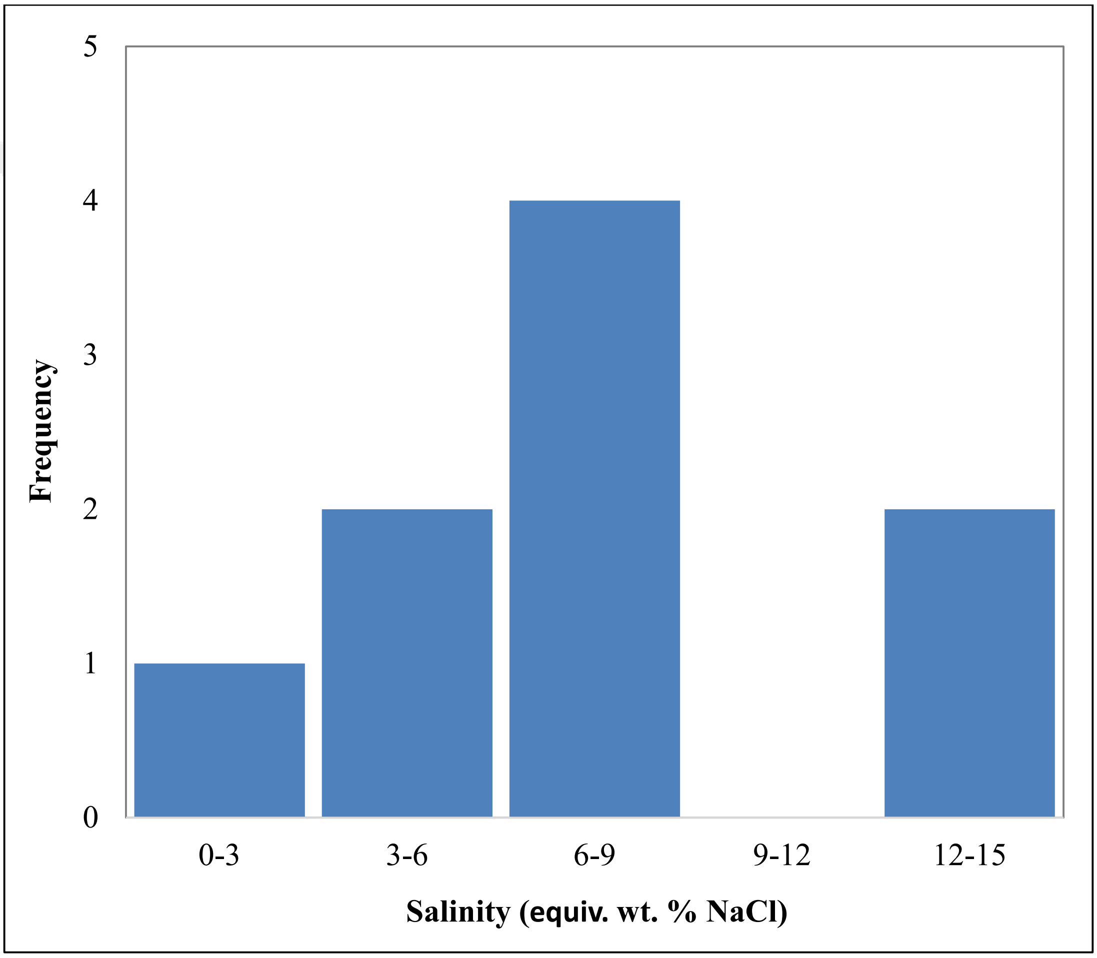

Figure 6.2 : Frequency histogram of the salinity values for the primary inclusions.

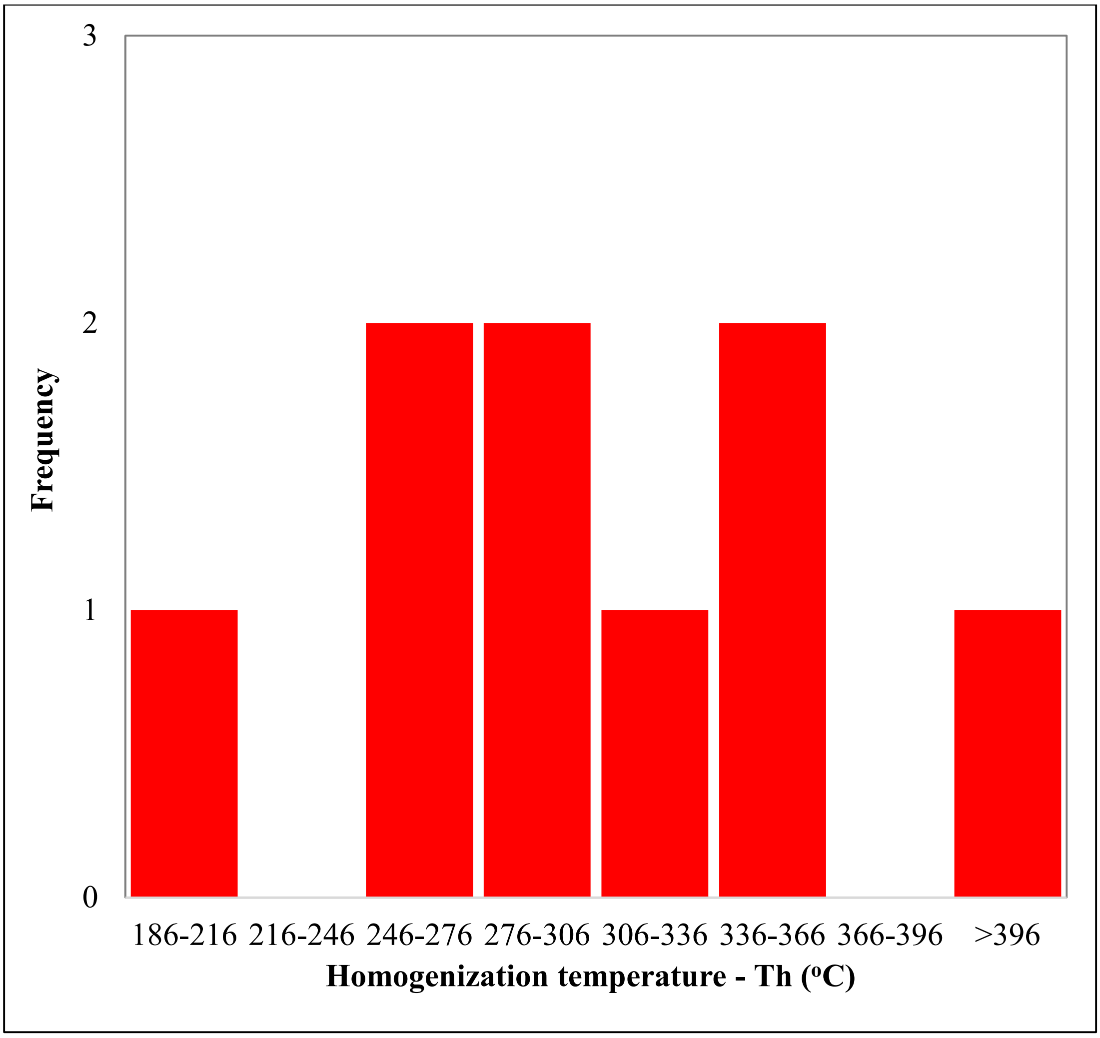

Figure 6.3 : Frequency histogram of the homogenization temperatures for the primary inclusions.

6.4 Boiling Trend

Crawford and Hollister (1986) purport that the fluids in the metamorphic rocks move through the fractures differing in size from microcracks to veins, and the planes of the secondary inclusions seem to mend these troughs. In other words, if the fluid derives during the generation of the inclusions by the expulsion of volatile matters from a solid and is in balance with the mineral assemblage of the host rock, it is very likely that these inclusions bear identical characteristics as the primary inclusions originated over the course of mineral development. Hence, T_h – Salinity diagram is presented in Figure 6.4, involving both primary and secondary inclusions. It can be deduced from the diagram that the fluid chemistry and temperature show a rapid change and that a probable retrograde boiling event occurs at low temperatures (~ 140 °C) alongside high and low salinty contents.

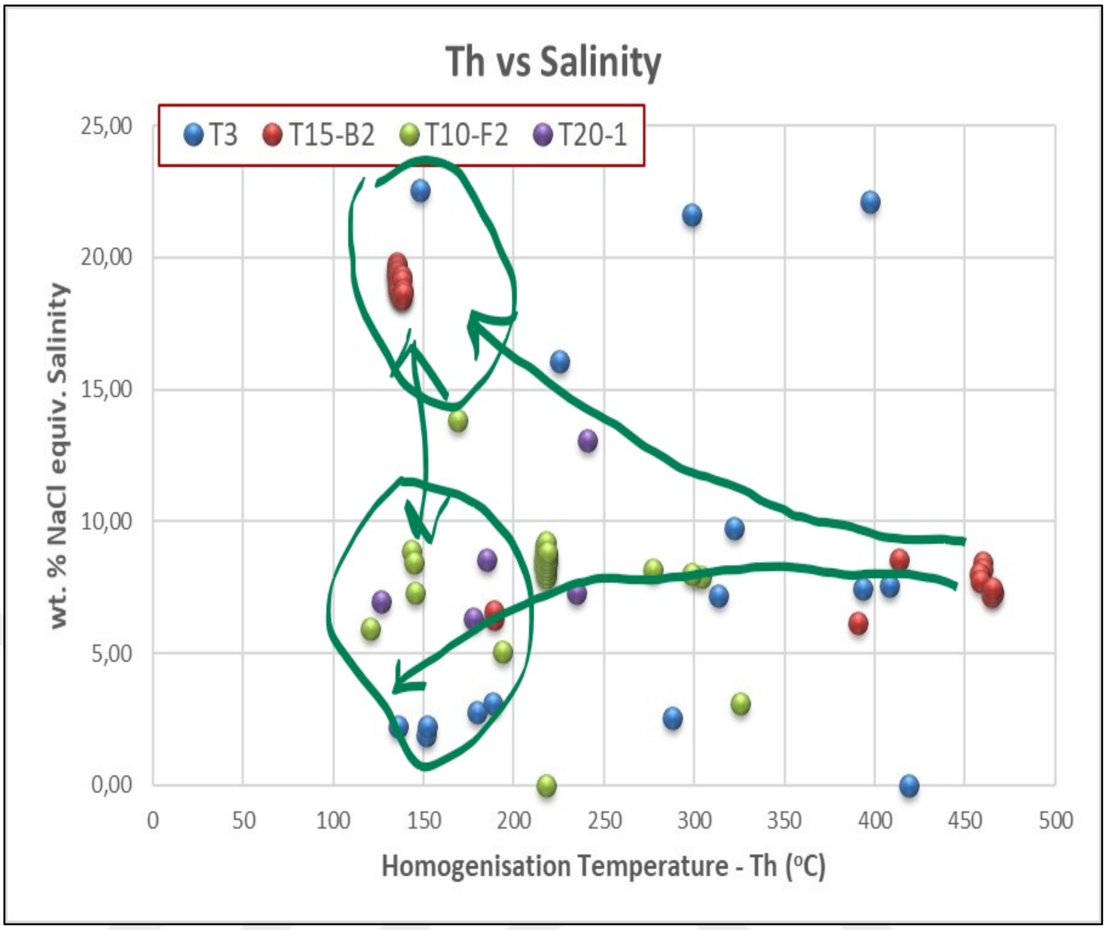

Figure 6.4 : Homogenization temperature (T_h) versus salinity diagram of both primary and secondary fluid inclusions of the Blagojev Kamen deposit. Note that the measurement results from the last quartz sample T10-3 which is of clathrate gas inclusions is not included.

6.5 Estimations of Fluid Pressure-Density-Depth

For the purpose of determining the fluid pressure, density and depth using the calculated mean T_h and NaCl factors for the primary inclusions, the thermal profiles correlated with vapor pressures and densities from Haas (1971) have been made reference to. The average homogenization temperature (~ 278 ºC) and salinity (7.32 wt. % NaCl) values of the Blagojev Kamen deposit are equivalent to ≈ 695 m, ≈ 61 bar (6.1 MPa) and ≈ 0.82 g/cm^3, respectively.

7. DISCUSSION

7.1 Metallogenic Properties of the Grabova Reka (Blagojev Kamen) Deposit

Blagojev kamen is located in the eastern part of Serbia, near the border with Romania and regarded as part of the Homolje-Beljanica metallogenic zone, situated west of the TMC (Timok Magmatic Complex). Majority of rocks in this location belong to the Proterozoic metamorphic units of Eastern Serbia, with historically noted wolfram/gold-wolfram/gold-silver-wolfram occurrences and deposits. Ore deposit type is chiefly of granitic veins and stockworks with traces of tin-wolfram mineralization, and occasioanally with copper, bismuth, antimony and variable amounts of placer gold. These veins are intruding throughout the mafic volcano-sedimentary sequence and Precambrian Greenstone Series and are principally 0.2 cm to 1.1 m in width, extending up to 100-200 m in longitude (Janković, 1982). Signs of pyritization are noticeable all over the vein mineralizations. Host rock lithology is in most scenarios introduced by chlorite schist and chloritic schist of an igneous origin, and by meta-volcanoclastics (meta-volcano-sedimentary).

Gold ± scheelite deposits close to Blagojev Kamen, also known as Grabova Reka, do have economic value. A great many quartz-gold veins with scheelite are found in early Paleozoic mafic volcano-sedimentary complex as green schist. Ore veins are embedded along the foliation of the schist (Figure 7.1.a). Native gold and scheelite are observed as the major ore minerals, with minor pyrite (occasionally present in green schist) and subordinate sphlalerite, galena and scarce pyrargyrite keeping them company (Figure 7.2.b). Controversially, primary gold is thought to be of volcano-sedimantary origin (Jelenković et al., 2002).

The Grabova Reka deposit comprises three nest-shaped gold-bearing quartz veins of hydrothermal origin in green schists within a 300 m wide fault zone. The precipitation of gold in the fractures is closely interconnected to its displacement across the green schist facies because of its exposure to metamorphism (Kalenić et al., 1980). The granitoid intrusions that cross-cut through the green schist facies gave rise to the energy transition required for the displacement of the hydrothermal fluids in question

(Janković, 1990). Generally, hydrothermal deposits related to volcano–intrusive complexes, hydrothermal metasomatic veins, porphyry–Cu and stockwork–disseminated–Mo types can be tracked. The prominent metals in these deposits are Pb–Zn, Sb, Bi, Ag, As. Gold-bearing sulfide mineralisation is copious while wolfram (scheelite) amounts to relatively less quantities (Jelenković et al., 2008).

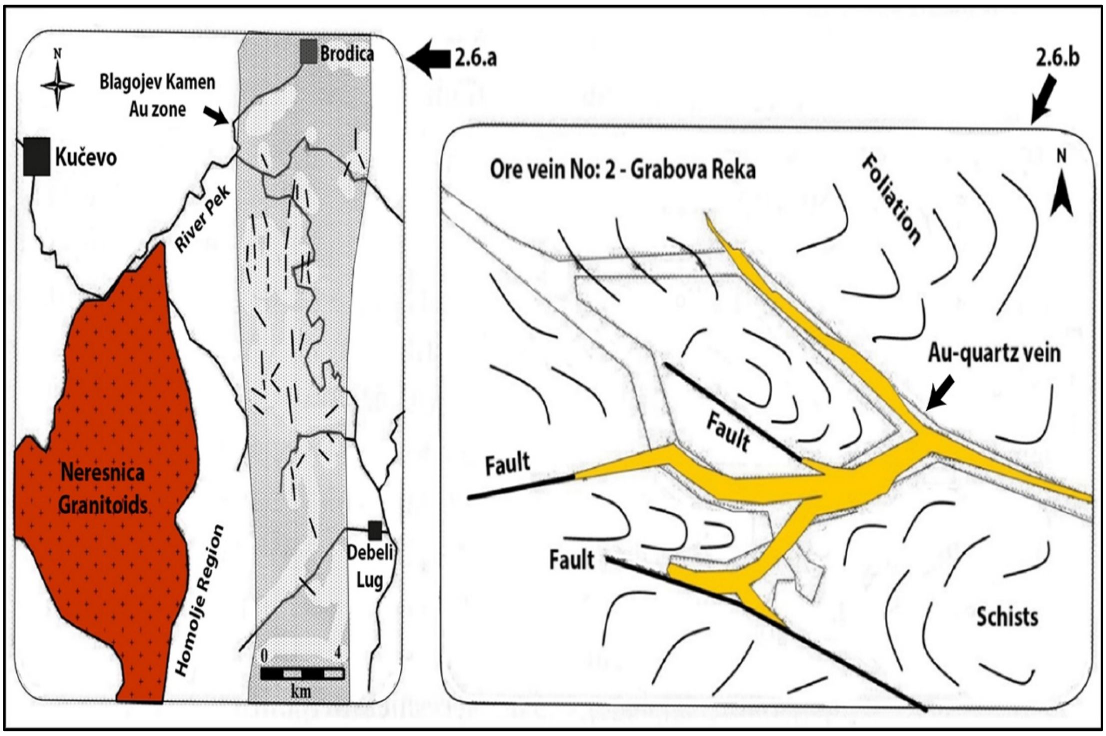

Figure 7.1 : (a) Location of the Blagojev Kamen ore-bearing structure with indicated places of particular ore veins; (b) Peculiar Au-bearing quartz vein in the scope of Blagojev Kamen ore-bearing area (modified after Jelenković et al., 2002).

Quaternary deposits in the Pek river unveil consequential alluvial gold accumulation and presence of monazite in the placer formed on the Neresnica granitoid (Jelenković et al., 2002). It is mentioned in the literature that the source of the gold alluvial placers has been derived and transported from the quartz veins of the Blagojev Kamen ore field.

7.2 Relation to the Epigenetic Model of the Mesothermal Systems

Kerrich and Fryer (1979) investigated the Au mesothermal systems of the Porcupine district in the Abitibi belt, and distinguished at least two stages of Au metallogeny. One of them referes to the existence of Au in carbonate-chert chemical sediments, which form in the lower mafic volcanic sequence. The other one is related to Au in hydrothermal quartz veins which evidently points to epigenetic occurrence in the greenstone sequence. The model, represented in Figure 7.2, suggests that the metamorphic fluids originate during burial and prograde metamorphism of the greenstone sequences (Pirajno, 1992).

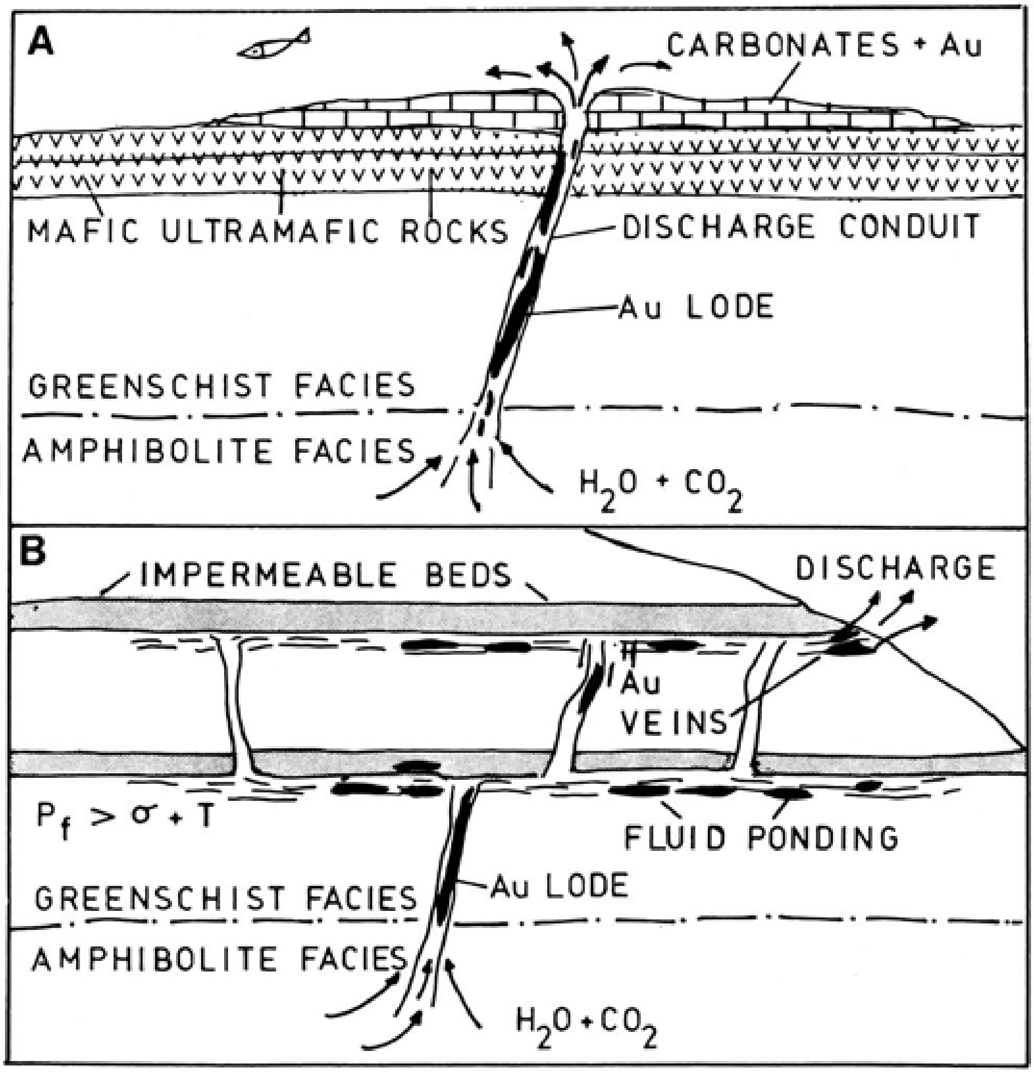

Figure 7.2 : A schematic of the epigenetic-syngenetic model of Kerrich and Fryer (1979). a) Accumulation and culmination of fluids at the sea floor; b) concentration and ponding of fluids below impermeable beds with sideward ejection. The drawing is not to scale.

Pirajno (1992) reasons that at the greenschist-amphibolite transition - between 450 and 500° C - about 5% dehydration H_2O and other volatiles are liberated from the mafic rocks. The surrounding conditions are in a way that the pressure of the metamorphic fluids, amplified by thermal extension of pore fluids, surpasses the litho-static pressure. The fluids concentrate along, and into structural channels (e.g. microcracks and fractures) where auriferous quartz veins are developed.

Kerrich and Fryer (1979) suggest that the residence time and gathering of the metamorphic fluids in the crust are measured by rates of fluid build-up and discharge, and for the Archean geothermal gradients were elevated (ca. 90°C km^{-1}), fluid formation would have exceeded expulsion. As it so happened, it would have resulted in the ponding of the fluids underneath impermeable layers as demonstrated in Figure 7.2. Whenever the fluid pressure surpasses the total horizontal stress along with the tensile strength of the rock, subvertical hydraulic fracturing happens, hereby allowing the expulsion of the fluids from the ponded reservoir. Hydraulic fractures are inclined to spreading towards the surface and the process of expulsion and ponding might take place a couple of times below the successive impermeable layers in the sequence. Fluids may discharge laterally or vertically from the reservoir into fractured conduits and cracks caused by faulting (Figure 7.2) in order to precipitate Au-bearing quartz-albite-tourmaline as veins at or adjacent to an unconformity (Pirajno, 1992).

8. CONCLUSIONS AND RECOMMENDATIONS

This study has ultimately developed an insight into various perspectives of the Blagojev Kamen deposit:

1- The findings indicate that the hydrothermal veins and stockworks that cross-cut the greenstone facies and the meta-volcanosedimantary units must have enriched the quartz minerals to some degree with diffused wolfram-tin-gold ore assemblages, despite the fact that no amount of gold has been traced whereas wolfram and tin contents showed only little to no economic importance based on the geochemical analysis results of the samples.

2- According to the macro- and microscopic observations made on the samples, a transition from phyllic (sericitic) to argillic type of hydrothermal alteration has been noted, along with propylitic and potassic alterations in part.

3- A trend of P-T increase in the metamorphic facies towards the south of the studied area has been manifested. The prograde metamorphic sequence demonstrated temperatures ranging from 400 to 700 ^{o}C and pressures from 4 to 12 kbar.

4- The manganese dioxide ore mineral ‘pyrolusite’ has been discovered in the ore petrographic study, also verified by the XRD and ICP-MS profiles. The ICP-MS results showed manganese valueing up to 1600 ppm and the other elements yielded concentrations of very little to no economic importance, demonstrating contents of wolfram up to 41 ppm, lithium 20,50 ppm, tin 3,20 ppm and tantalum 2,65 ppm in bulk. It is also thought that the sampled specimens are contaminated with Pb due to the proximate Variscan granitoid intrusions in the vicinity.

5- Stable isotope analyses demonstrated different environment types for the fluid generation. $\delta^{34}S$ and $\delta^{18}O$ isotope analyses revealed that the sulphide minerals are of an igneous origin and the water is affiliated to the metamorphic genesis.

6- Approximate mineralization temperature, pressure and depth values have been estimated with the fluid inclusion applications confirming the literature-backed concepts related to the depositon and mineralization characteristics of the Blagojev Kamen ore field. Average homogenization temperature indicates low to intermediate crystallization temperature environments with reasonably low salinities Plus, the clathrate – CO_2 gas entrapments found in the inclusions have been elaborated.

In terms of determining the profitability (economically desired grade gram/ton) and feasilibility of the Blagojev Kamen W-Au deposits, more detailed and sophisticated analyses such as SEM (Scanning Electron Microscope), TEM (Transmission Electron Microscope), EPMA (Electron Probe Microanalyzer), Raman Spectroscopy, etc. should be conducted in the future on the collected quartz vein samples along the alteration zones. A closer look into fluid inclusion studies is recommended that be made on biotite minerals in favor of garnering precise data on the mineralization temperature and domain of the wolfram-gold ore bodies.

REFERENCES

Anzulović, A. (2022). *Mineralogical and geochemical study of the metamorphic rocks from the the W-Au deposit Blagojev Kamen, Serbia* (Master thesis). University of Zagreb, Faculty of Mining Geology and Petroleum Engineering, ZAGREB.

Balen, D., Horváth, P., Tomljenović, B., Finger, F., Humer, B., Pamić, J., Árkai, P. (2006). A record of pre–Variscan Barrovian regional metamorphism in the eastern part of the Slavonian Mountains (NE Croatia). *Mineralogy and Petrology, 87 (1)*, p. 143–162.

Balla, Z. and Bodrogi, I. (1993). The'Vékény Marl Formation'of Hungary. *Cretaceous Research, 14 (4–5)*, p. 431–448.

Bodnar, R.J. (1993). Revised equation and table for determining the freezing point depression of H2O-NaCl solutions. *Geochimica et Cosmochimica Acta, 57,* p. 683-684.

Borojević Šoštarić, S., Palinkaš, A.L., Neubauer, F., Cvetković, V., Bernroider, M., Genser, J. (2014). The origin and age of the metamorphic sole from the Rogozna Mts., Western Vardar Belt: New evidence for the one–ocean model for the Balkan ophiolites. *Lithos, 192*, p. 39–55.

Cassard, D., Bertrand, G., Maldan, F., Gaàl, G, Juha, K. (2012). ProMine Pan-European Mineral Deposit Database: A New Dataset for Assessing Primary Mineral Resources in Europe. Nancy, France.

Channell, J.E.T. and Horvath, F. (1976). The African/Adriatic promontory as a palaeogeographical premise for Alpine orogeny and plate movements in the Carpatho–Balkan region. *Tectonophysics, 35 (1–3)*, p. 71–101.

Craig, H. (1961). Isotopic Variations in Meteoric Waters. *Science*, *133,* p. 1702–1703.

Crawford, M.L. and Hollister, L.S. (1986). Metamorphic Fluids: The Evidence from Fluid Inclusions. *Springer, 5,* p. 1-35. doi: 10.1007/978-1-4612-4896-5_1.

Csontos, L. (1995). Tertiary tectonic evolution of the Intra–Carpathian area: a review. *Acta Vulcan, 7 (2)*, p. 1–13.

Csontos, L. and Vörös, A. (2004). Mesozoic plate tectonic reconstruction of the Carpathian region. *Palaeogeogr, Palaeocl, 210,* p. 1–56. doi: 10.1016/j.palaeo.2004.02.033.

Csontos, L., Nagymarosy, A., Horváth, F., Kovac, M. (1992). Tertiary evolution of the Intra–Carpathian area: a model. *Tectonophysics*, 208 (1–3*)*, p. 221–241.

Cvetković, V., Prelević, D., Schmid, S. (2016). Geology of south–eastern Europe. P. Papić (Ed.): Mineral and thermal waters of Southeastern Europe: *Springer*, p. 1–29.

Darling, R.S. (1991). An extended equation to calculate NaCl contents from final clathrate melting temperatures in H2O-CO2-NaCl fluid inclusions. *Geochimica et Cosmochimica Acta, 55,* p. 3869-3871.

Delibaş, O., Moritz, R., Ulianov, A., Chiaradia, M., Saraç, C., Revan, K.M., Göç, D. (2016a). Cretaceous subduction-related magmatism and associated porphyry-type Cu–Mo prospects in the Eastern Pontides, Turkey: New constraints from geochronology and geochemistry. *Elsevier, 248-251*, p. 119–137.

Dimitrijević M.D. (1982). Dinarides: An outline of the tectonics. *Earth Evolution Sci., 1,* p. 4-23.

Dimitrijević M.D. (1997). Geology of Yugoslavia. *Geological Institute – GEMINI, Belgrade, Spec. Publ., Monograph,* p. 1-197.

Fülöp, J. (1989). Introduction to geology of Hungary. Bevezetés Magyarország geológiájába (in Hungarian).

Gallhofer, D., Quadt, A., Peytcheva, I., Schmid, M.S., Heinrich, C.A. (2015). Tectonic, magmatic, and metallogenic evolution of the Late Cretaceous arc in the Carpathian-Balkan orogen. *Advancing Earth and Space Science Publications, 34,* p. 1813-1836. doi: 10.1002/2015TC003834.

Haas, J.L. (1971). The Effect of Salinity on the Maximum Thermal Gradient of Hydrothermal System at Hydrostatic Pressure. *Economic Geology*, *66*, p. 940-946.

Haas, J.L., Császár, G., Kovács, S., Vörös, A. (1990). Evolution of the western part of the Tethys as reflected by the geological formations of Hungary: Acta Geodetica Geophysica et Montanistica Hungarica, v. 25: Akademiai Kiado, Budapest.

Haas, J.L. and Péró, C. (2004). Mesozoic evolution of the Tisza Mega–unit. *International Journal of Earth Sciences, 93 (2)*, p. 297–313. doi: 10.1007/s00531–004–0384–9.

Haydoutov, I. (1989). Precambrian ophiolites, Cambrian island arc, and Variscan suture in the South Carpathian–Balkan region. *Geology, 17 (10)*, p. 905–908.

Higgins, N.C. (1980). Fluid inclusion evidence for the transport of tungsten by carbonate complexes in hydrothermal solutions. *Can. J. Earth Sci., 17*, p. 823-830.

Hoefs, J. (1987). Stable Isotope Geochemistry. Springer-Verlag. Berlin Heidelberg.

Iancu, V., Berza, T., Seghedi, A., Marunţiu, M. (2005). Palaeozoic rock assemblages incorporated in the South Carpathian Alpine thrust belt (Romania and Serbia): a review. *Geologica Belgica*.

Janković, S. (1967). Metallogenic epoch and ore areas of Yugoslavia. Faculty of Mining and Geology, Belgrade (in Serbian).

Janković, S. (1974). Metallogenic provinces of Yugoslavia in time and space. In Janković S. (Ed.), *Metallogeny and concepts of the geotectonic evolution of Yugoslavia*. (pp.37-63, in Serbian). Faculty of Mining and Geology, Belgrade (in Serbian).

Janković, S. (1982). Yugoslavia. In Dunning F.W., Mykura W. & Slater D. (Eds.). *Mineral deposits of Europe* (Vol. 2, pp.143-198). Southeast Europe. Mineral. Soc. Inst. of Mining and Metallogeny.

Janković, S. (1990). The ore deposits of Serbia: Regional metallogenic settings, environments of deposition, and types. Faculty of Mining and Geology, Belgrade, 760 (in Serbian, with a summary in English).

Janković, S. (1997). The Carpatho-Balkanides and adjacent area: a sector of the Tethyan Eurasian metallogenic belt. *Mineralium Deposita, 32,* p. 426-433.

Jelenković, R., Serafimovski, T., Tasev, G. (2002). Metallic mineral resources of the Karpatho-Balkan metallogenic province: Eastern Serbian Sector (general review). *RMZ – Materials and Geoenvironment, 49*, p. 177-197.

Jelenković, R., Kostić, A., Životić, D., Ercegovac, M. (2008). Mineral resources of Serbia. *Geologica Carpathica, 59*, p. 345-361.

Jovanović, D., Cvetković, V., Erić, S., Kostić, B., Peytcheva, I., and Šarić, K. (2019). Variscan granitoids of the East Serbian Carpatho-Balkanides: new insight inferred from U-Pb zircon ages and geochemical data. *Swiss Journal of Geosciences*, *112*, p. 121–142.

Kalenić, M. and Hadži–Vuković, M. (1978). Basic Geologic Map of SFRY 1:100000, Sheet Kučevo. Veselinović, M. O., Rakić, B., Vujisić, Č., Lončarević, M., Navala, M., Đorđević, M., Vasiljev, N., Banković, V.: Zavod za geološka, hidrogeološka, geofizička i geotehnička istraživanja, Beograd.

Kalenić, M., Hadži–Vuković, M., Dolić, D., Lončarević, Č., Rakić, M.O. (1980). Explanatory book for sheet Kučevo, Basic Geological Map of SFRY 1:100.000, p. 53.

Karamata, S. (2006). The geological development of the Balkan Peninsula related to the approach, collision and compression of Gondwanan and Eurasian units. *Geological Society, London, Special Publications, 260 (1)*, p. 155–178.

Kerrich R. and Fryer B. J. (1979) Archaean precious-metal hydrothermal systems, Dome Mine, Abitibi greenstone belt. II. REE and oxygen isotope relations. Can J Earth Sci 16:440-458

Knežević, V., Cvetković, V., Resimić, K., Memović, E., Živković, P. (1997). Wall-rock alterations and their significance for the Pb, Zn and Cu ore deposits investigation in Serbia. In Romić K., Kondžulović R. (Eds.). *Ore deposits exploration* (pp.28-32). Faculty of Mining and Geology, Belgrade (in Serbian).

Kovács, S. (1984). Tisia–probléma és lemeztektonika. *Földt. Kut, 27 (1)*, p. 55–72.

Kounov, A., Seward, D., Bernoulli, D., Burg, J–P, Ivanov, Z. (2004). Thermotectonic evolution of an extensional dome: the Cenozoic Osogovo–Lisets core complex (Kraishte zone, western Bulgaria). *International Journal of Earth Sciences, 93 (6)*, p. 1008–1024.

Kovács, S., Császár, G., Galácz, A., Haas, J., Nagy, E., Vörös, A. (1989). The Tisza Superunit was originally part of the North Tethyan (European) margin. *Evolution of the northern margin of Tethys. Mem. Soc. Geol. France, 154 (4)*, p. 81–100.

Kräutner, H.G. and Krstić, B.P. (2003). Geological map of the Carpatho–Balkanides between Mehadia. In *Oravita, Niš and Sofia*.

Krstekanić, N., Stojadinović, U., Kostić, B., Toljić, M. (2017). Internal structure of the Supragetic Unit basement in the Serbian Carpathians and its significance for the late Early Cretaceous nappe–stacking. *Geoloski anali Balkanskoga poluostrva, 78*, p. 1–15.

Krstić, B. and Karamata, S. (1992). Terranes of the Serbian Carpatho–Balkanides. *Comptes Rendus des Seances de la Soc. Serb. de Geol., livre jubilaire (1891—1991)*, p. 57–74.

Moritz, R., Rezeau, H., Ovtcharova M., Tayan R., Melkonyan R., Hovakimyan S., Ramazanov V., Selby D., Ulianov A., Chiaradia M., Putlitz B. (2016). Long-lived, stationary magmatism and pulsed porphyry systems during Tethyan subduction to post-collision evolution in the southernmost Lesser Caucasus, Armenia and Nakhitchevan. *Gondwana Research, 37*, p. 465–503.

Oczlon, M.S., Seghedi, A., Carrigan, C.W. (2007). Avalonian and Baltican terranes in the Moesian Platform (southern Europe, Romania, and Bulgaria) in the context of Caledonian terranes along the southwestern margin of the East European craton. *SPECIAL PAPERS–GEOLOGICAL SOCIETY OF AMERICA, 423*, p. 375.

Parker, R. (2017). Pyrolusite - Stealth Manganese. *The Rocky Mountain Association of Geologists, 66*, p. 34-43.

Pamić, J., Balen, D., Herak, M. (2002). Origin and geodynamic evolution of Late Paleogene magmatic associations along the Periadriatic–Sava–Vardar magmatic belt. *Geodinamica Acta, 15 (4)*, p. 209–231. doi: 10.1080/09853111.2002.10510755.

Pirajno, F. (1992). *Hydrothermal Mineral Deposits: Principles and Fundamental Concepts for the Exploration Geologist.* Springer Berlin, Heidelberg.

Prinz, G. (1926). Geography of Hungary. I. In *The origin, structure and form of the earth of Hungary (in Hungarian). Tud Gyujt, 15*, p. 1–200.

Richards, J.P. (2014). Tectonic, magmatic, and metallogenic evolution of the Tethyan orogen: From subduction to collision. *Ore Geology Reviews, 70,* p. 323-345.

Săndulescu, M. (1994). Overview on Romanian geology. *Rom. Jour. of Tectonics and Regional Geology, Suppl., 2, 75*, p. 3–15.

Schmid, S.M., Bernoulli, D., Fugenschuh, B., Matenco, L., Schefer, S., Schuster, R., Tischler, M., Ustaszewski, K. (2008). The Alpine-Carpathian-Dinaridic orogenic system: Correlation and evolution of tectonic units. *Swiss Journal of Geosciences, 101*, p. 139–183.

Seghedi, A., Berza, Tudor, I., Viorica, M., Marcel, OAIE, G. (2005). Neoproterozoic terranes in the Moesian basement and in the Alpine

Danubian nappes of the South Carpathians. *Geologica Belgica, 8 (4)*, p. 4–19.

Sharp, Z.D. and Kirschner, D.L. (1994). Quartz-calcite oxygen isotope thermometry: A calibration based on natural isotopic variations. *Geochimica et Cosmochimica Acta*, *58*, p. 4491-4501.

Singer, D.A., Berger, V.J., Moring, C. (2008). *Porphyry Copper Deposits of the World: Database and Grade and Tonnage* (Report No: 2005 – 1060) U.S.A. : U.S. Geological Survey Open-File Report.

Spahić, D., Gaudenyi, T., Glavaš–Trbič, B. (2019). The Neoproterozoic–Paleozoic basement in the Alpidic Supragetic/Kučaj units of eastern Serbia: a continuation of the Rheic Ocean?. *Acta Geologica Polonica, 69 (4)*.

Taylor, H.P., Jr. (1974). The Application of Oxygen and Hydrogen Isotope Studies to Problems of Hydrothermal Alteration and Ore Deposition. *Economic Geology, 69*, p. 843-883.

APPENDICES

APPENDIX A : Simplified geological map of Kučevo
APPENDIX B : X-ray diffractograms

APPENDIX A

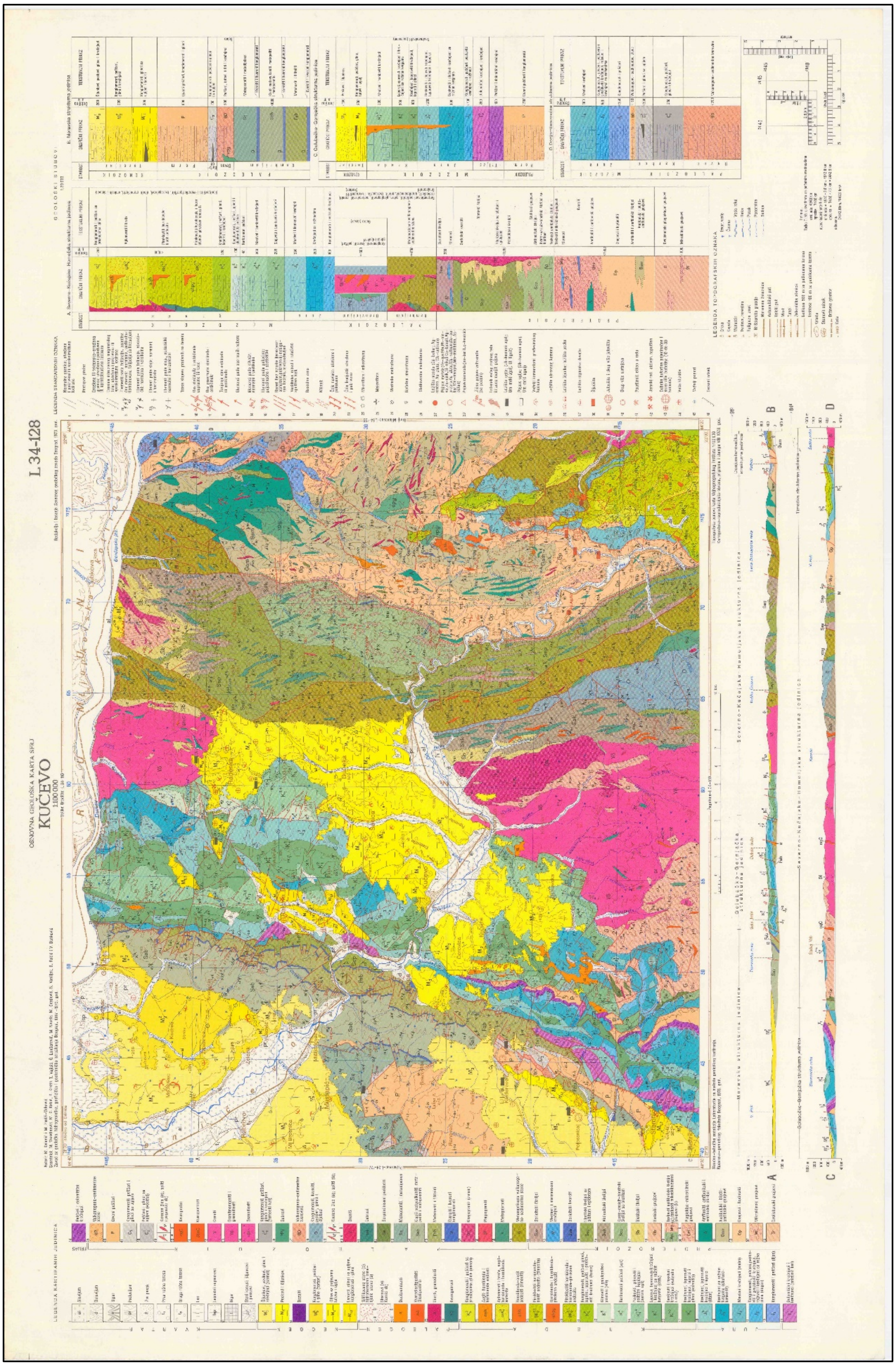

Figure A.1 : Simplified 1:100.000-scale geological map of Kučevo (Kalenić and Hadži–Vuković, 1978).

APPENDIX B

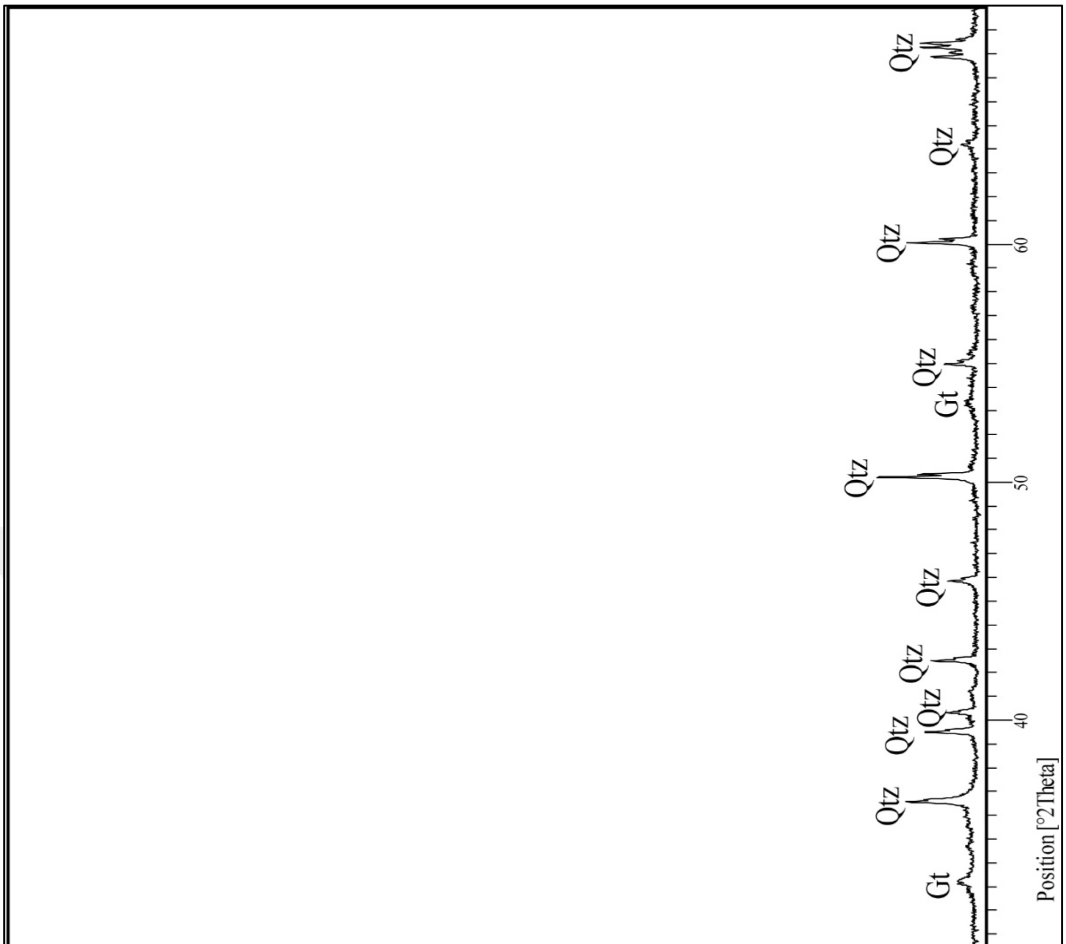

Figure B.1 : X-ray diffractogram of the sample 7554.

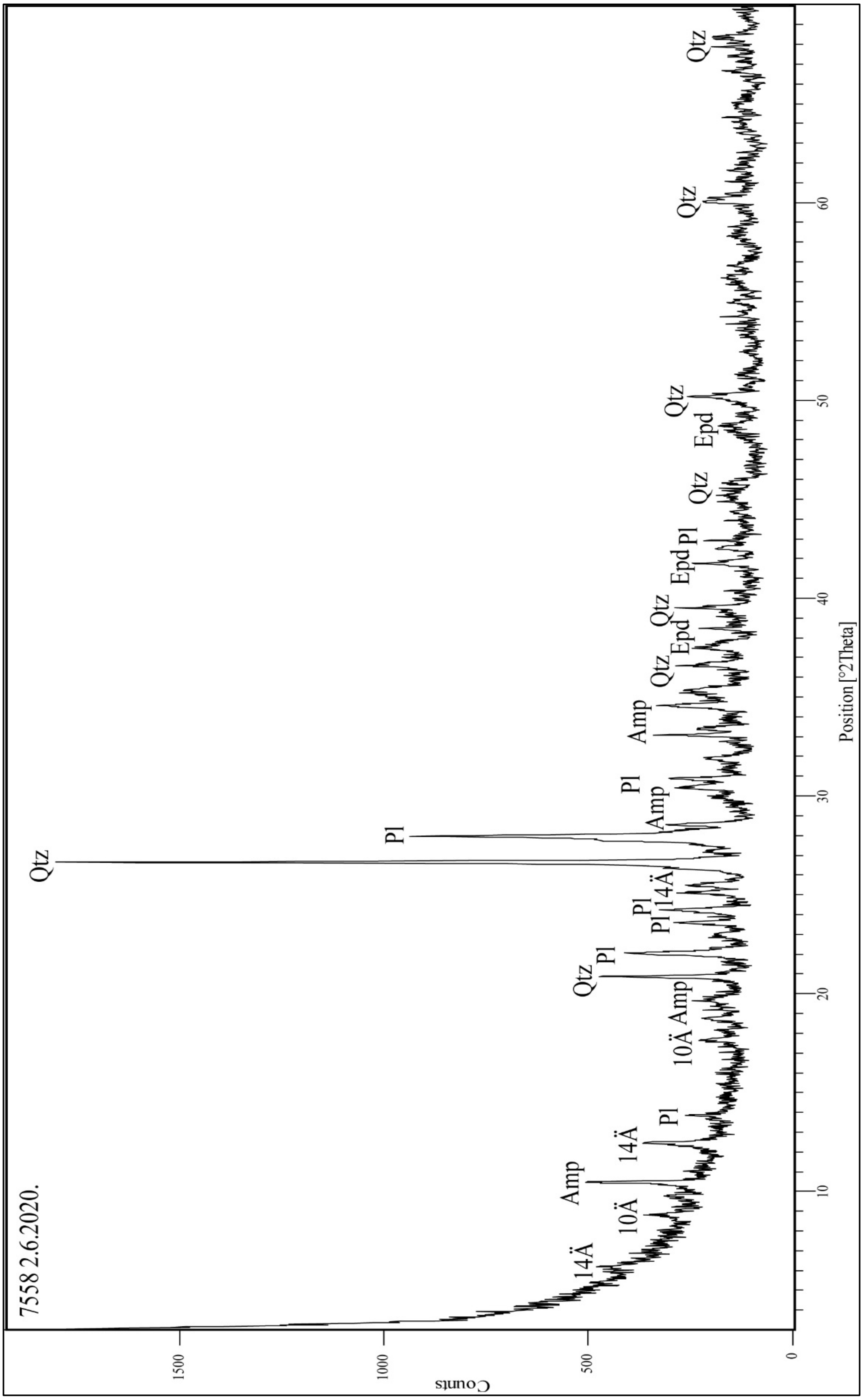

Figure B.2 : X-ray diffractogram of the sample 7558.

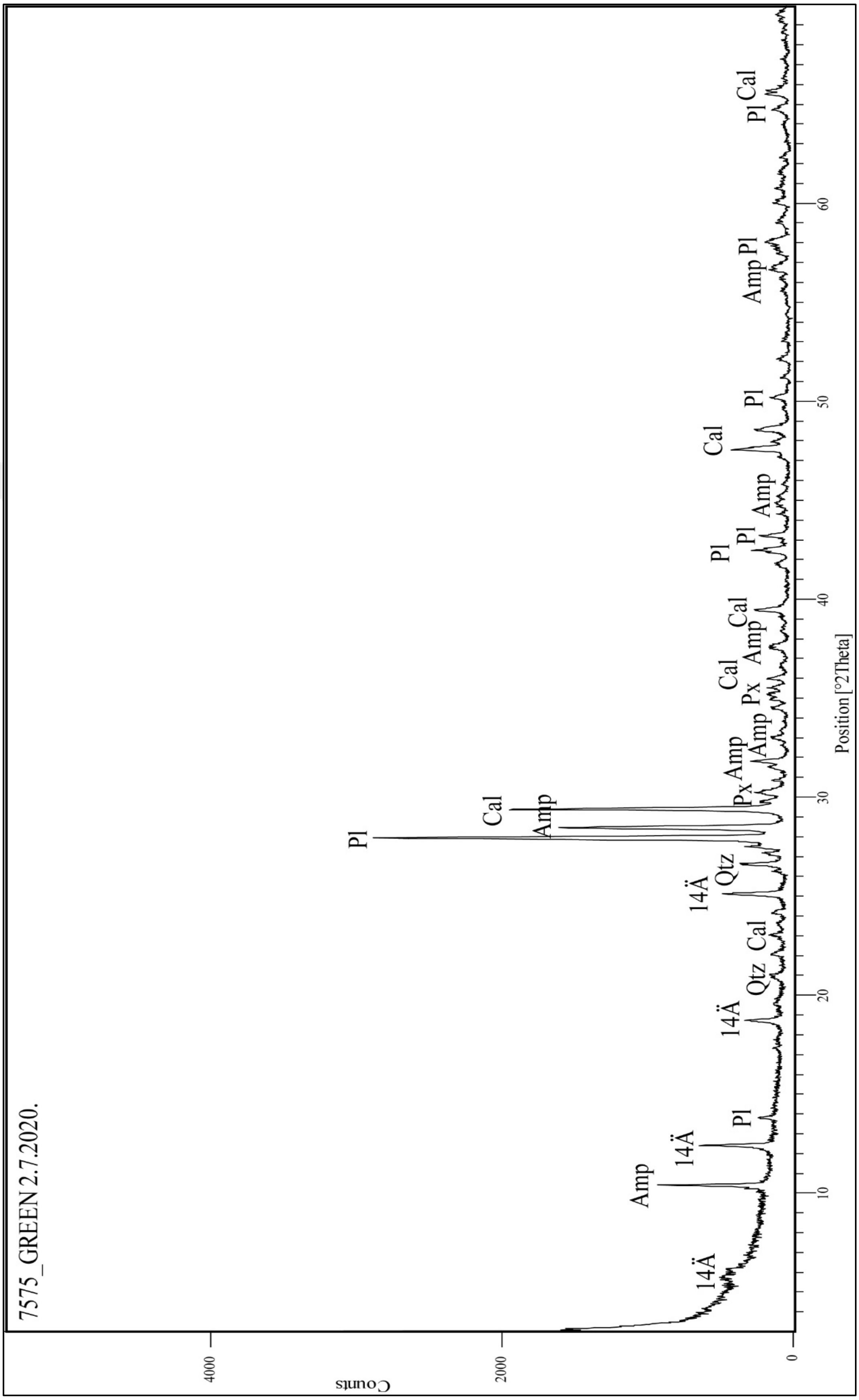

Figure B.3 : X-ray diffractogram of the sample 7575 (green).

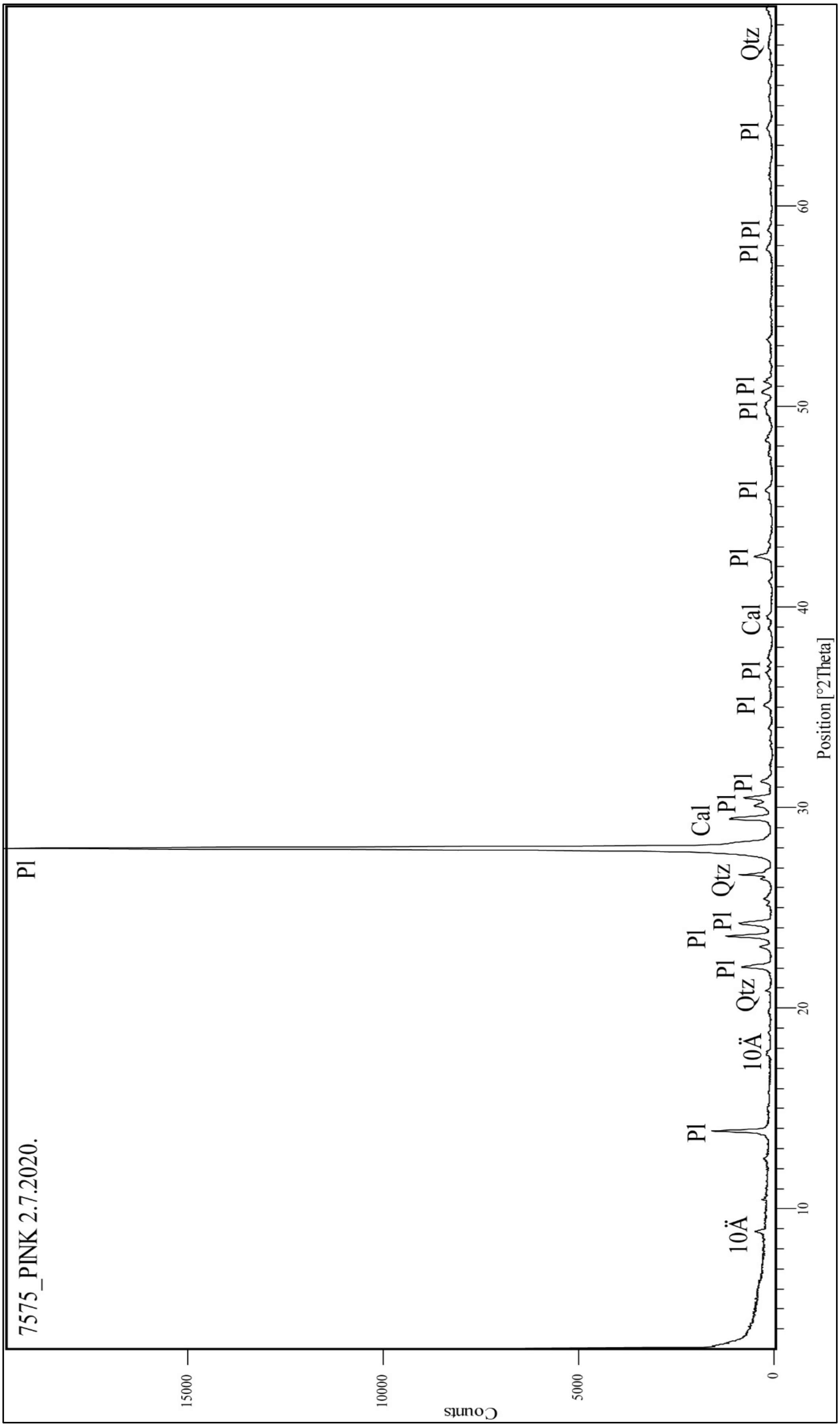

Figure B.4 : X-ray diffractogram of the sample 7575 (pink).

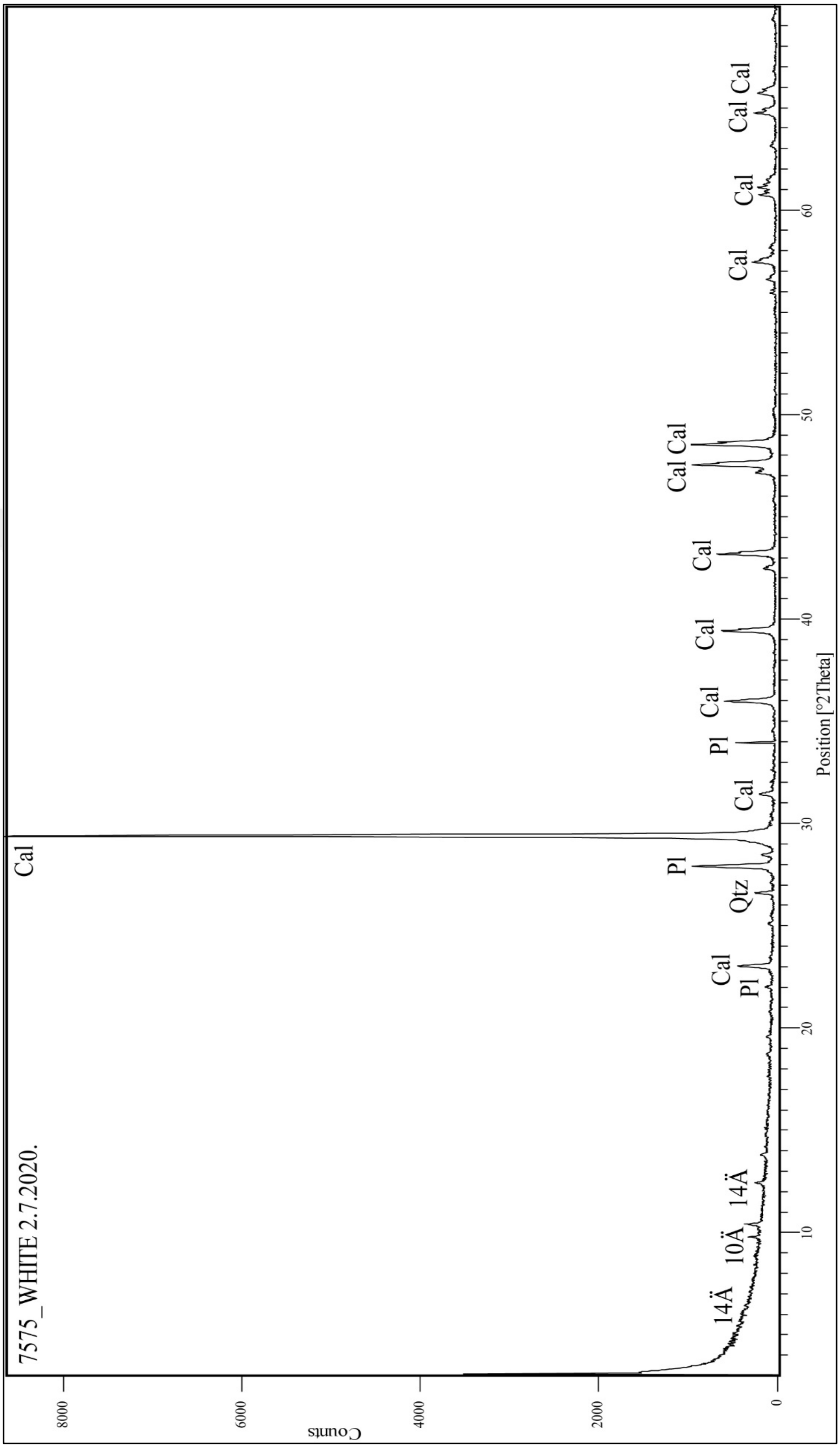

Figure B.5 : X-ray diffractogram of the sample 7575 (white).

CURRICULUM VITAE

Name Surname : **Berk BAŞER**

EDUCATION :

- **B.Sc.** : 2018, Eskişehir Osmangazi University, Faculty of Engineering and Architecture, Department of Geological Engineering

PROFESSIONAL EXPERIENCE:

- (2016) Lab intern at the University of Castilla-La Mancha, Ciudad Real/Spain
- (2018) Engineering intern at Üç Eksen Zemin Sondaj, Eskişehir/Turkey
- (2018) Engineering intern at Koza Gold Corporation, Izmir/Turkey
- (2021 – Present) Field Engineer at Geolog International B.V., Ankara/Turkey